UNIVERSITA' DEGLI STUDI DI PADOVA

Sede Amministrativa: Università degli Studi di Padova

Dipartimento di Biologia

SCUOLA DI DOTTORATO DI RICERCA: BIOCHIMICA E BIOTECNOLOGIE
INDIRIZZO: BIOTECNOLOGIE
CICLO XXI

VAMP7: a model system to study the Longin Domain-SNARE motif.

Direttore della Scuola : Ch.mo Prof. Giuseppe Zanotti
Supervisore :Ch.mo Prof. Francesco Filippini

Dottorando : Sandro Vivona

Index

Abstract

Eukaryotic cells rely on a complex system of membrane-enclosed compartments that are maintained by the trafficking of shuttling vesicles. The fusion of these vesicles with the target compartment relies on multiprotein complexes that have been conserved throughout eukaryotic evolution. SNARE (soluble N-ethylmaleimide-sensitive factor attachment protein receptor) proteins are considered the engine of membrane fusion in all trafficking pathways of the cell. Upon specific protein-protein interactions, SNARE proteins that are localized in opposing membranes form a four helix bundle that releases free energy and induces membrane fusion. The SNARE motif is the elementary unit of this bundle and defines all SNARE proteins.

SNARE proteins possess other regulatory domains that contribute in modulating the specificity of the fusion event. One of these accessory elements is the Longin Domain (LD). Other than being well conserved among all eukaryotes, the LD is not limited to SNAREs only and is present in many molecular processes related to the life cycle of vesicles. LD-containing SNAREs are called Longins and are divided in three main subfamilies: Ykt6p, Sec22b, VAMP7. The Longin Domain (LD) is usually composed of about 120 amino acids arranged in a globular structural fold that consists of five β strands (β1- β5) sandwiched by one α helix (α1) on one side and two helices (α2 and α3) on the other side.

The LD can fold back onto the SNARE motif in Ykt6p and Sec22b but not in Nyv1p – a fourth minor longin subfamily. This intramolecular interaction involves a surface-exposed hydrophobic pocket contributed by the α1-β3 structural elements, which is bound by the SNARE motif. This mechanism eventually inhibits and prevents unspecific formation of the SNARE complex, thus regulating the vesicle fusion process.

However, very little is known about the dynamic properties of such mechanism. The present study uses VAMP7 as a model system to reveal these characteristics. Our interest in VAMP7 relies on the fact that not only VAMP7 lacks any direct evidence of the LD-SNARE interaction, but it also offers a system of natural variations to the usual LD-SNARE domain arrangement that can prove extremely useful in our study. The present work reveals unknown dynamic properties of the LD-SNARE interaction supporting a dominantly “closed conformation” for Longins, with heterogeneous characteristics. The results shown in this research complement well with what we already know about a similar auto-inhibitory mechanism observed in the Syntaxin subfamily of SNAREs. Therefore, we provide here new bases for a better understanding of the regulatory mechanisms involved in vesicle fusion.

Riassunto

Le cellule eucariote sono caratterizzate da un complesso sistema di membrane, che offre svariate compartimentazioni con diverse condizioni chimico-fisiche. Se da una parte tale sistema permette la realizzazione di un'ampia gamma di processi biochimici, dall'altra richiede un altrettanto complesso sistema di interscambio atto al suo mantenimento. Tale interscambio è assicurato dal trafficking di vescicole che originano da un compartimento donatore e riversano il loro contenuto in un compartimento accettore attraverso un processo che richiede la fusione delle membrane lipidiche. Tale processo si fonda sull'organizzazione di complessi macromolecolari a cui contribuiscono varie famiglie proteiche ben conservate attraverso l'evoluzione eucariotica. La famiglia delle SNARE è una di queste. Le SNAREs sono considerate i motori della fusione di membrane. La loro capacità di formare complessi specifici in *trans* tra le due memrane su cui risiedono fornisce il contributo energetico necessario a indurre la fusione degli strati lipidici. Tali complessi consistono in un intreccio di quattro eliche chiamate SNARE motifs, domini di circa 60-70 amino acidi che definiscono tutte le SNAREs.

Oltre allo SNARE motif, le SNAREs contengono spesso domini accessori a funzione regolativa. Uno di questi è il Longin Domain (LD). Il LD non è limitato alle sole SNAREs e anzi si ritrova in altre famiglie proteiche tutte coinvolte in processi molecolari riguardanti il ciclo vitale di una vescicola. Nelle SNAREs, il LD definisce una famiglia chiamata Longins, suddivisa a sua volta nelle proteine Ykt6, Sec22b e VAMP7. Il LD consiste di circa 120 aminoacidi organizzati in una struttura spaziale globulare che comprende un piano di cinque foglietti β (β1- β5), complessati da un'alfa elica (α1) su un lato e da altre due eliche (α2-α3) sull'altro.

In Ykt6 e Sec22b si è dimostrata la possibilità che il LD si ripieghi sullo SNARE motif e lo coordini su una sua superficie idrofobica compresa tra α1 e β3. Questo meccanismo si è dimostrato in grado di prevenire la formazione di complessi SNARE non specifici. Tuttavia ben poco si conosce ad oggi sulla natura di questa interazione in termini dinamici, a differenza di quanto invece si sa per un analogo meccanismo osservato nella famiglia SNARE delle Sintaxine. In altri temrini non è dato sapere se nelle Longine questo meccanismo implica una conformazione stabilmente "chiusa" di LD e SNARE, o se piuttosto esso si realizza come un equilibrio dinamico tra conformazioni aperte e chiuse. Una serie di motivi, tra cui l'assenza di dati diretti per questo fenomeno in VAMP7 e la possibilità di usufruire di sue varianti naturali, ci hanno spinto a scegliere VAMP7 come sistema modello per fornire le risposte ai suddetti interrogativi.

I nostri dati suggeriscono per le Longine una conformazione stabilmente chiusa, ma non omogenea e capace di cambi conformazionali molto rapidi. Questo lavoro complementa bene quanto già noto

per le sintaxine e fornisce dunque la possibilità di comprendere meglio i meccanismi regolativi gneralmente adottati nella fusione vescicolare.

Introduction

Traffic and vesicle fusion

Eukaryotic cells have evolved a sophisticated system of membrane-enclosed compartments that is a hallmark of their complexity. Compartmentalization offers functional and spatial partitioning into different specific organelles, each with its own specific and functional biochemical environment. Transport between these organelles in the endocytic and exocytic pathways is mediated by shuttling vesicles that carry cargo proteins. These vesicles bud and selectively recruit cargo from a donor compartment. They then target an acceptor compartment into which they transfer their load upon docking and fusion of the membranes [Bonifacino and Glick, 2006].

In spite of the notable heterogeneity of the endomembrane system, budding and fusion of trafficking vesicles relies on multiprotein complexes that consist of protein families that have been well conserved throughout evolution.

This thesis focuses on the SNARE (soluble N-ethylmaleimide-sensitive factor attachment protein receptor) protein superfamily, which plays a central role in vesicle membrane fusion [Jahn & Scheller, 2006]. In general, a membrane fusion process – either in the endocytic or exocytic pathway – can be roughly divided into five main steps, as shown in **figure 1** [Wickner and Schekman, 2008]. First, membranes are brought to close proximity ("tethering") by the interplay of at least three classes of proteins: (i) Membrane-anchored Rab GTPase proteins, (ii) Rab effectors, that bind active GTPases and stimulate GTP hydrolysis, and finally (iii) tether proteins, that usually consist of long coiled-coil structures functioning as a path guiding the vesicle (**figure 1a**). The membrane region where Rab is anchored is then enriched with lipids and proteins that are specific to the fusion process. This Rab-mediated recruitment includes the SNARE proteins (**figure 1b**). In most instances, trans-SNARE complex forms between 4 SNARE motifs, 3 from the acceptor membrane and the fourth from the donor (**figure 1c**). Many details have yet to be unravelled regarding the number of accessory proteins taking part in this mechanism and interfering with the SNARE complex (see the next paragraph for more details). SNAREs the free energy to drive the hemifusion of the outer halves of each membrane, with the inner halves and the luminal contents still separated at this point (**Figure 1d**). Final mixing of the inner lipid layer and luminal content completes the fusion, with the SNARE complexes that now are in a *cis* state. Finally, the cis complex is disassembled apart by the AAA-ATPase protein NSF (N-ethylmaleimide-sensitive factor) upon α-SNAP (soluble NSF attachment protein) binding (**figure 1e**). Exocytosis is a well studied membrane fusion process. This is true for neuronal synapses in particular, as they have become a model for vesicle fusion research, due to their high exocytic activity, high content of fusion proteins and high interest in human brain.

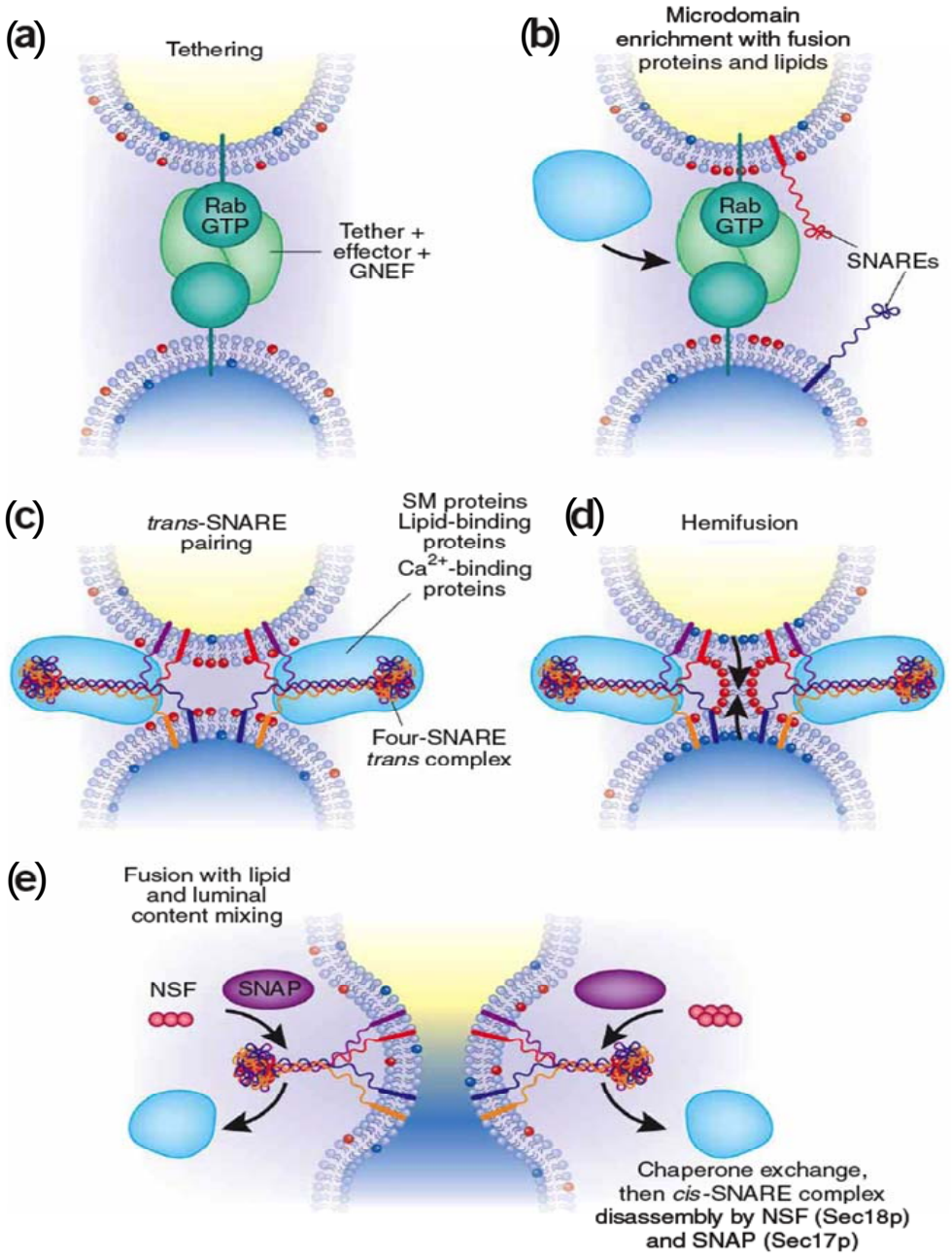

Figure 1 (from Winker and Scheckman, 2008). A generic vesicle fusion event of the endocytic or exocytic pathway, divided in five phases: **(a)** Two membranes approach each other thanks to tethering proteins bound by a membrane-anchored complex of an activated GTPase (Rab) with its cognate effector; **(b)** Rab-mediated enrichment of both lipids and proteins (red and blue molecules) necessary to fusion **(c)** formation of trans SNARE complexes with accessory proteins, such as Sec/Munc (SM) proteins, Ca2+- and/or lipid-binding proteins; **(d)** fusion of only the outer halves of the two lipid bilayers (hemifusion), with the next lipid movement indicated by black arrows; **(e)** mixing of lipid bilayers, membrane proteins and luminal compartments complete the fusion, with the SNARE complexes (now in *cis* state) that are ready to be disassembled by α-SNAP and NSF.

Exocytosis is a well studied membrane fusion process. This is true for neuronal synapses in particular, as they have become a model for vesicle fusion research, due to their high exocytic activity, high content of fusion proteins and high interest in human brain. Synaptic vesicles have

shown to release neurotransmitters using two types of exocytosis pathways: a slow, asynchronous and constitutive process and a fast Ca^{2+}-triggered membrane fusion that is synchronous with the action potential arrival. Unlike constitutive and mostly intracellular fusion events, fast fusion relies on a pre-fusion state, in which several vesicles are already docked and primed to fuse to the cell membrane, awaiting the Ca^{2+}-mediated trigger.

SNARE proteins and SNARE complex

SNAREs are considered the engines of membrane fusion [Jahn and Scheller, 2006]. Their importance became clear when the group of Cesare Montecucco in Padova discovered that *clostridium* neurotoxin proteases target SNAREs for neurotransmission disruption [Schiavo et al., 1992]. Since then, a remarkable scientific effort has produced great knowledge in the field. SNAREs are a superfamily of small proteins conserved in eukaryotes with quite simple domain architecture. The SNARE motif, a conserved stretch of 60-70 amino acids arranged in heptad repeats, is the defining domain of all SNAREs. Usually, a single transmembrane region at the C-terminus of the SNARE motif anchors the molecule to the membrane, but there are cases in which this is achieved via post-translational modification such as palmitoylation. Finally, as we discuss below in more details, either unstructured, short stretches or extended, folded domains can be present at the N-terminus [Dietrich et al., 2003; Brunger, 2005]. The initial assumption that mutually exclusive compartments possess different SNAREs led to the "v-SNARE" (vesicle SNARE) and "t-SNARE" (target SNARE) classification. However, it is possible that v- and t-SNAREs are not strictly separated (v-SNAREs of a certain pathway can be t-SNAREs of another). Further, this nomenclature is also inappropriate when considering homotypic fusions. A more precise classification emerged from fine structural properties of the neuronal SNARE complex, whose crystal structure was solved by the group of Axel Brunger in a milestone study [Sutton et al., 1998]. SNAREs are either R-SNAREs or Q-SNAREs, according to the presence of either an arginine or a glutamine in a key, conserved position in the SNARE motif. This position is also called the "ionic layer" or "zero layer" as it sets a central frame register for the four assembling SNARE motifs. Indeed, the formation of the complex implies a disorder-to-order transition of the SNARE motifs such that a parallel four-helix bundle is composed of 16 primarily hydrophobic layers formed by interacting side-chains from each of the four α-helices (see **figure 2).** Along with this nomenclature, it was proposed that all fusion-competent SNARE complexes arise from the contribution of 3 Q- (Qa, Qb, Qc) and 1 R-SNARE motif [Fasshauer et al., 1998].

Roughly speaking, v- and t-SNAREs usually coincide with R- and Q-SNAREs and it can often be

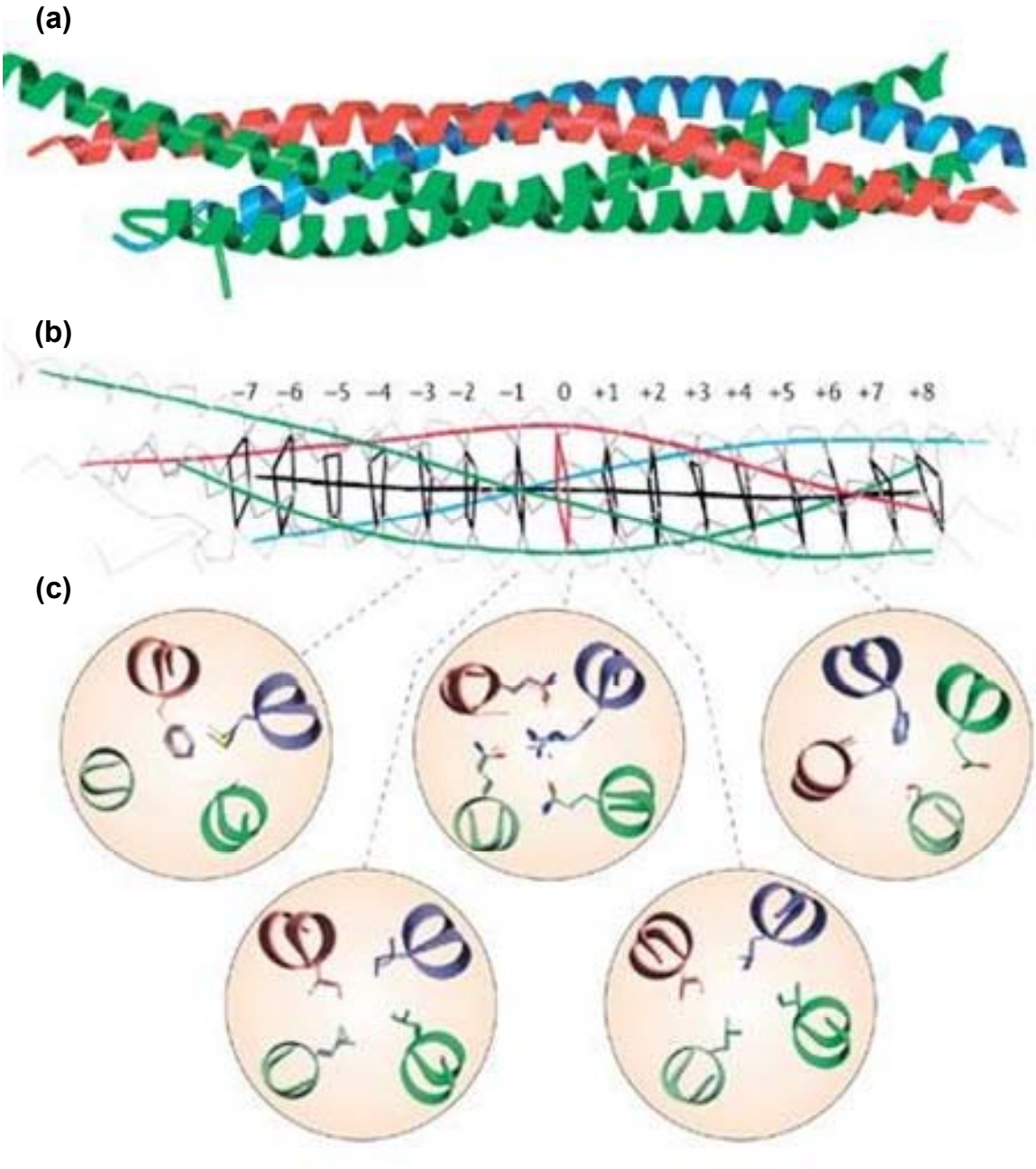

Figure 2 (adapted from Jahn and Scheller, 2006). Molecular structure of a SNARE complex. **(a)** Crystal structure of the neuronal SNARE complex: SNARE motifs of Syntaxin 1 (red), SNAP25 (green) and Synaptobrevin II (blue), all oriented with their N-termini on the left; **(b)** Skeleton representation of the inner layers of interacting side chains, numbered and coloured with black contours (except the ionic layer in red), with the Cα backbones shown in grey and the helical axes coloured as in panel a; **(c)** Close up view of the structures (ribbon representation) of single layers in shaded circles: the 3 upper circles show the highly asymmetric layers -3, 0 and +6, whereas the two lower ones represent the highly hydrophobic layers surrounding the 0 layer.

convenient and intuitive to use the v-/t- nomenclature. In the neuronal SNARE complex, Qa is contributed by Syntaxin1A (hereafter referred to as simply Syntaxin), Qb and Qc by SNAP25A (synaptosome-associated protein of 25 kDa, hereafter referred to as simply SNAP25) and finally R

by Synaptobrevin II (hereafter referred to as simply Synaptobrevin). However, due to their amphiphilic nature, SNARE motifs can also associate in other combinations that result in helical bundles that are less stable than core complexes and that demonstrate a notable conformational and oliogomeric variability of SNAREs [Brunger, 2005; Jahn and Scheller, 2006].

Syntaxins contain an N-terminal independently folded domain, the Habc domain, which is connected to the SNARE motif by a short linker. The Habc domain is a three helix bundle, which is able to fold back on the SNARE motif to form a four-membered coiled coil, thus giving the Syntaxin a closed conformation state. Besides binding to SNAP25 and Synaptobrevin through its SNARE motif, Syntaxin can bind Munc18-1; this interaction is incompatible with the SNARE complex and requires a closed state of Syntaxin. Recent evidence suggest that Munc18-1 binding stabilizes the Syntaxin closed conformation, thus inhibiting effect on the SNARE complex formation and membrane fusion, which heavily depends on this open/close conformational switch [Chen et al., 2008; Gerber et al., 2008]. SNAP25 contributes 2 SNARE motifs to the neuronal SNARE complex – Qb and Qc. An unstructured linker separates them and anchors the molecule to the membrane through palmitoylation. However, in non-neuronal fusion Qb and Qc can be contributed by single-motif t-SNAREs [Brunger 2005]. Finally, neuronal Synaptobrevin has a short unstructured N-terminal region that can be missing in other synaptobrevins. In 2001 however, a new class of R-SNAREs, defined by a synaptobrevin-homolog SNARE motif and a longer and independently folded N-terminal domain titled Longin Domain (LD), *vide infra* [Filippini et al., 2001].

Longin Domain and Longins

The Longin Domain (LD) was discovered and defined by a bioinformatic study [Filippini et al., 2001]. The group of Francesco Filippini in Padova identified this N-treminal, conserved region of about 120 amino acids in the sequences of some vesicle associated membrane proteins (VAMPs) and termed it Longin Domain, in contrast with the short and variable N-terminal "brevin" regions known at that time. In the same year, the groups of Banfield and Scheller published the structures of the N-terminal domain of the yeast SNARE protein Ykt6 and the mouse SNARE Sec22b [Tochio et al., 2001; Gonzalez 2001]. As revealed by these structures, the LD fold consists of 5 antiparallel β-strands (β1-β5) sandwiched by an α-helix (α1) on one side and two helices (α2- α3) on the opposing side (see **figure 3**). Synaptobrevins are limited to bilateria, whereas longins are conserved in all eukaryotes and are classified in three major subfamilies based on homology to respectively VAMP7, Sec22b and Ykt6p [Rossi et al., 2004].

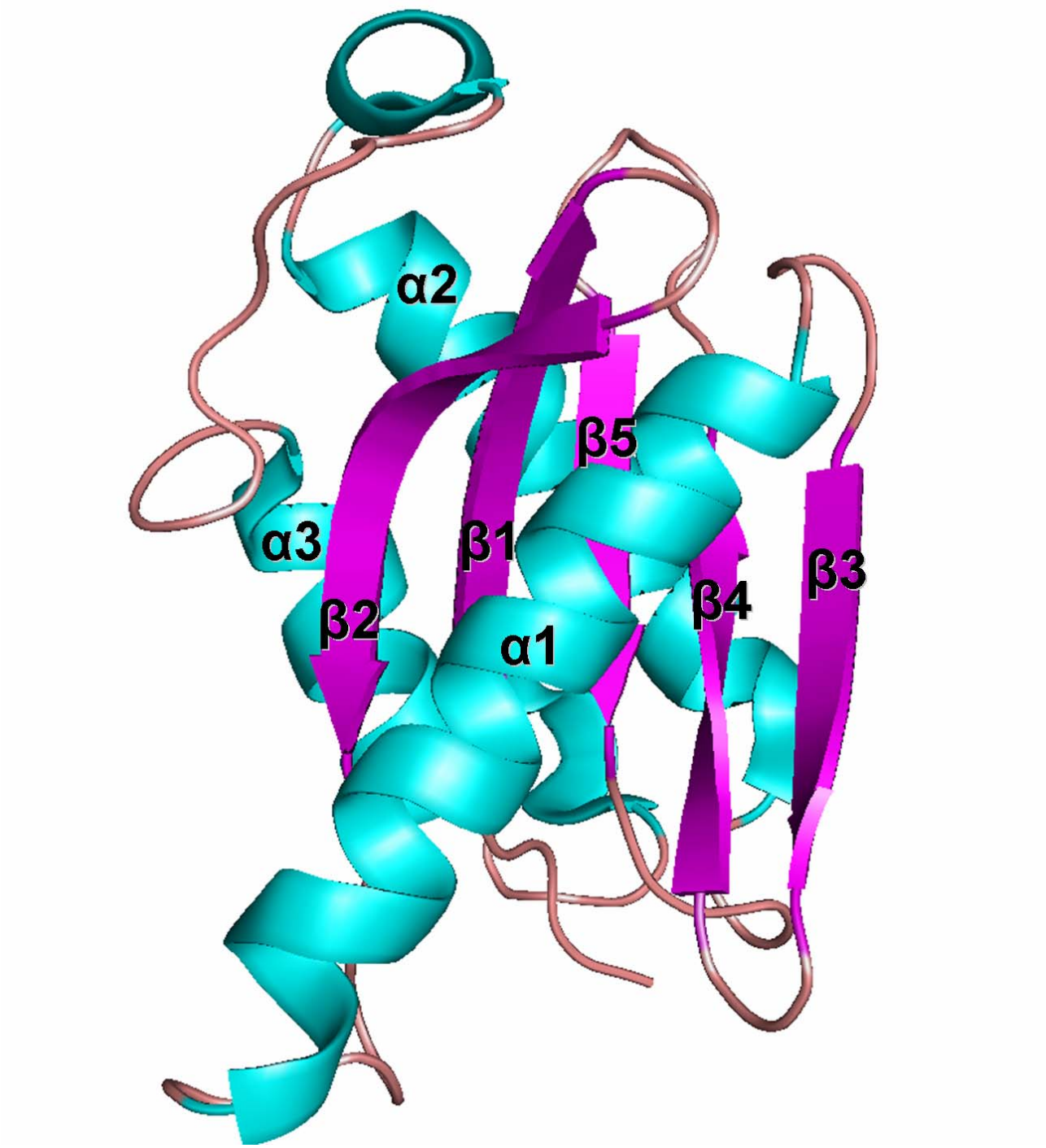

Figure 3. Ribbon representation of the NMR structure of the LD of Ykt6. Secondary structural elements are named from the N- to the C-terminus as β1-β2-α1-β3-β4-β5-α2-α3 and are coloured in cyan (α-helices) or purple (β-strands).

However, LDs are not limited to SNAREs. Surprisingly, a number of proteins related to trafficking pathways have been found to possess a longin-like fold domain. These include σ and μ subunits of the AP2 clathrin adaptor complex [Collins et al., 2002], the SRX subunit of the signal recognition particle receptor (SRP) [Schlenker et al., 2006] and the SEDL subunit of the TRAPP complex [Kim

et al., 2006]. Longin-like folds have been identified by *in silico* analyses also in CHiPS and DUF254 proteins [Kinch and Grishin, 2006]. It is striking to note the constant presence of a LD-like fold in the life cycle of a vesicle: from a protein machinery, such as the AP complex, dedicated to vesicle formation, to the TRAPP complex, mediating vesicle docking, finally to the SNARE complex, specialized in vesicle fusion. Even outside the vesicle life cycle, the LD has shown fascinating properties: the SRX subunit of the SRP receptor interacts with the small GTPase SRβ subunit, thus acting as its cognate effector and suggesting a role for the LDs as potential small-GTPase effectors [Schlenker et al., 2006]. This data collectively suggests the LD acts as a possible linkage between the structural components of vesicles (coats and SNAREs) and their regulatory machinery (small GTPases like Rabs, ARFs, ARLs, etc.), although many molecular and functional details are still to be unravelled [Edeling et al., 2006]. For this study we focus on the "longins" as defined above – i.e. R-SNAREs that comprise a LD.

LDs have been shown to regulate the targeting of R-SNAREs to the proper subcellular compartment. LD targets VAMP7 to late endosomes in mammals through an interaction with the δ-subunit of the AP3 complex [Martinez-Arca et al., 2003]. Plants have several different VAMP7 proteins, which are targeted to their different subcellular localizations by their LDs [Uemura et al., 2005]. In mammalian Ykt6 as well, only the LD confers the specialized localization, likely by masking other localization signals in the SNARE motif and chaperoning the prenylated C-ter of the protein [Hasegawa et al., 2003; Hasegawa et al., 2004]. The ability to bind lipid groups is confirmed by the Ykt6 LD-mediated palmitoylation of vac8 [Dietrich et al., 2004]. LD has also proved fundamental in selecting cargo into sorting vesicles through the interaction with vesicular coat proteins. Sec22b is exported from the endoplasmic reticulum (ER) to the Golgi due to an interaction between the α2-α3 interface of the LD and the COPII subcomplex Sec23/24. The SNARE motif plays a key role in this packaging as its N-terminal half folds on the α1-β3 interface of the LD and induces the creation of the conformational epitope on the α2-α3 surface, which is recognized by the Sec23/24 subcomplex. At the same time this folded back conformation would sequester the SNARE motif and prevent it to promiscuously bind unspecific partners [Mancias and Goldberg, 2007]. NMR (Nuclear Magnetic Resonance) data show an analogous LD-SNARE intramolecular interaction in Ykt6 [Tochio et al., 2001], but not in Nyv1 [Wen et al., 2006]. This mechanism then shows to be conserved to some extent among longins and it happened to prove dramatic in regulating the secretory pathway of Sec22b. VAMP7 showed some striking new insight about this important molecular mechanism, that is thoroughly investigated in this study (*vide infra*).

VAMP7: a model for LD-SNARE coexistence and interaction

VAMP7 is also known as tetanus insensitive VAMP (TI-VAMP) due to its resistance to tetanus and *botulinum* neurotoxins [Galli et al., 1998]. As a member of the longins/R-SNARE family, VAMP7 is involved in different membrane fusion processes within intracellular vesicle traffic (see **figure 4**).

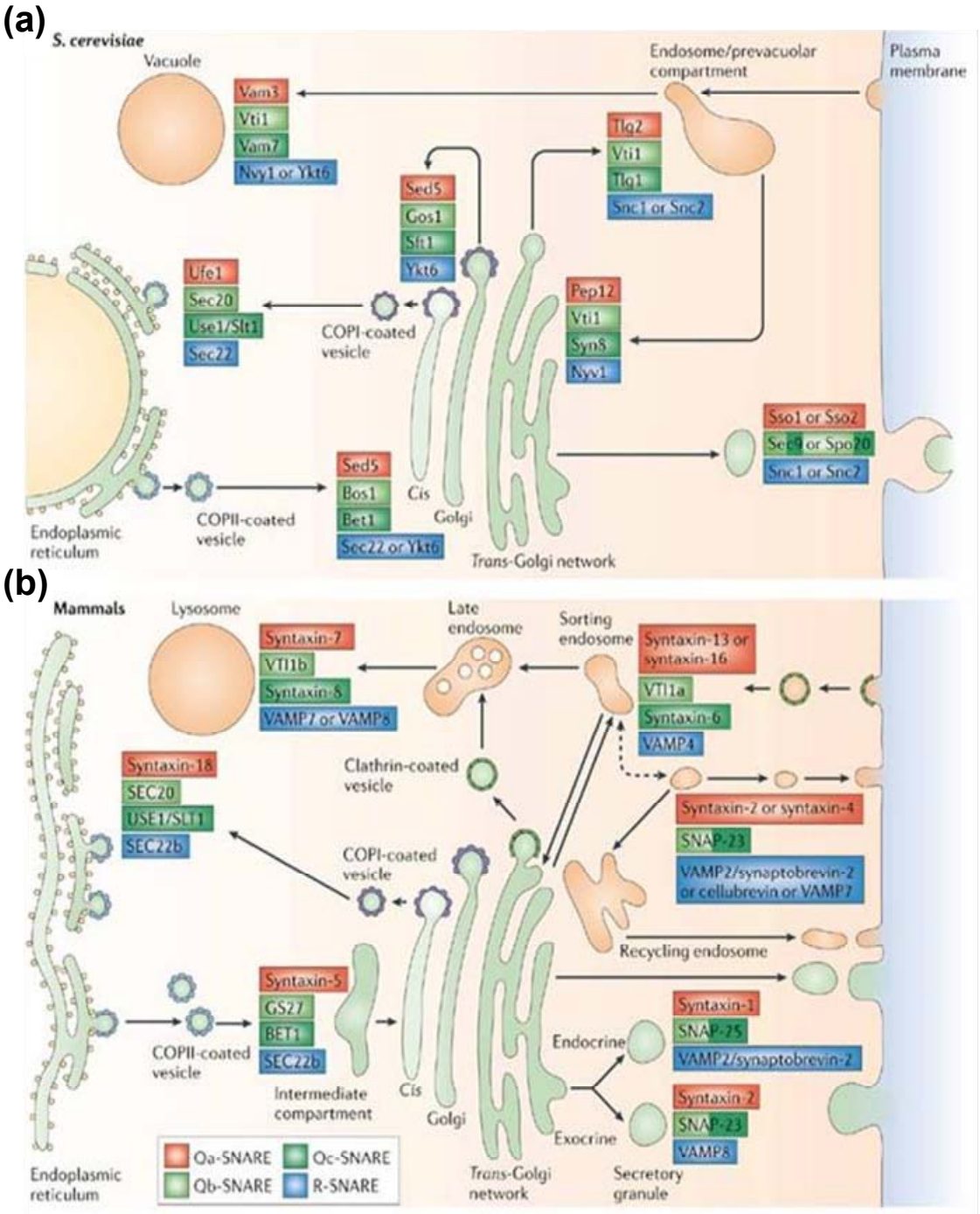

Figure 4. Assignment of the SNAREs involved in the membrane fusion events taking place in the different localizations of the secretory pathway of a yeast (a) or mammalian (b) cell.

In most non-neuronal cells VAMP7 localizes into late endosomes, this is followed by transport to lysosomes and the plasma membrane where it mediates the fusion of the endosome-derived vesicles [Advani et al., 1999; Luzio et al., 2007]. In neurons, VAMP7 is a component of synaptic vesicles

[Takamori et al., 2006] and a key player of neuronal morphogenesis; it localizes at the tips of axons and dendrites and is required for vesicular transport as part of mediating neuritogenesis [Alberts and Galli, 2003]. Interestingly, overexpression of VAMP7 LD inhibits neuritogenesis in neuroendocrine cells and both axonal and dendritic outgrowth in hippocampal neurons, whereas expression of an LD deletion mutant of VAMP7 increases the formation of SNARE complexes and strongly stimulates neurite outgrowth [Martinez-Arca et al., 2000; Martinez-Arca et al., 2001]. Other evidence strongly links VAMP7 to neuronal plasticity: VAMP7 mediates the transport of L1 – an important cell adhesion molecule (CAM) involved in axonal elongation – and the formation of L1-CAM-dependent cell contacts [Alberts et al., 2003]. This data collectively shows the importance of VAMP7 in neuronal morphogenesis. VAMP7's gene SYBL1 (Synaptobrevin-like 1) was the first X-linked gene to be found transcriptionally repressed on the pseudoautosomal region (PAR) of the Y chromosome [D'Esposito *et al*. 1996]. SYBL1 is expressed ubiquitously, both in human and in mouse tissues [D'esposito et al., 1996; Matarazzo et al., 1999], but its function appears very prominent in brain due to the strong linkage VAMP7 has with cellular morphogenesis and neuronal plasticity in particular. In this sense we like to observe that VAMP7 is the only longin R-SNARE that has been amplified in plants where morphogenesis is a constant challenge in these organisms' life: 12 VAMP7 genes in Arabidopsis thaliana in contrast with only 2 genes for Ykt6 and 2 for Sec22 [Rossi et al., 2004; Uemura et al., 2005]. Finally, a polymorphism in its regulatory region has suggested SYBL1 as one of the candidate genes for the bipolar syndrome disorder [Saito et al., 2000; Muller et al., 2002].

Besides the biological relevance of VAMP7 in brain and the potential outcome of eventual VAMP7-related disorders, another relevant feature captures our scientific interest: the SYBL1 splicing system. Two main SYBL1 splice variants have been predicted *in silico* and validated by real time-PCR and western blots of Jurkat cell extracts; the domain architecture of their protein products, VAMP7b and VAMP7c, is shown in **figure 5** [Vacca et al., in preparation]. VAMP7b originates from exon 6 skipping: this in turn results in a frameshifted sequence coding a new and longer protein C-terminus (starting at the 145th residue) and mutates the majority of the SNARE motif, including the ionic layer and the transmembrane domain. Instead, VAMP7c retains the main isoform's domain architecture but lacks 41 residues in the middle of the LD sequence, due to an in frame exon skipping.

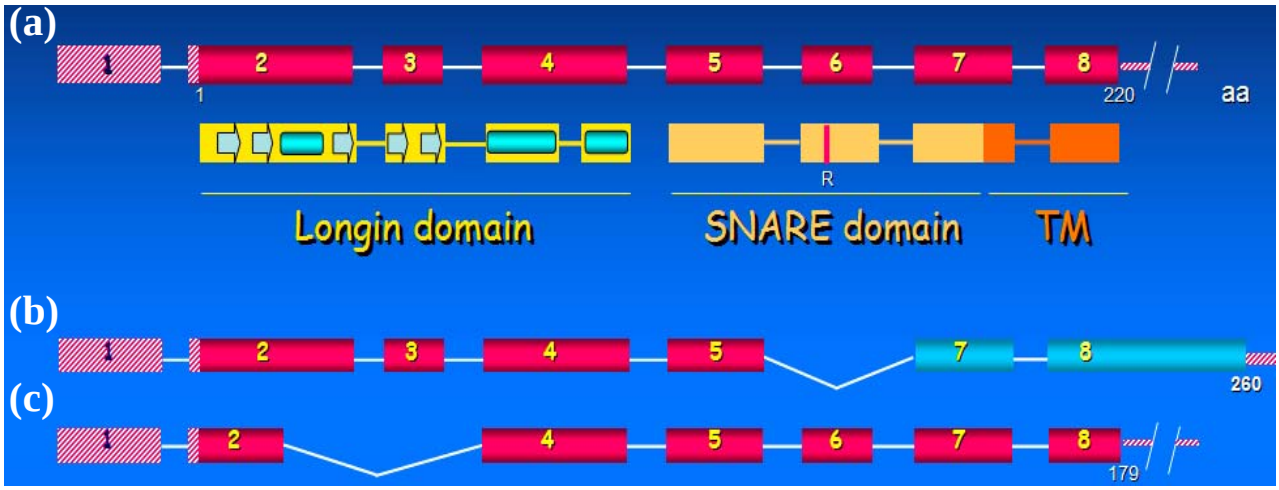

Figure 5. SYBL1 alternative splice variants. **(a)** Exon structure of the main isoform, SYBL1a. Untranslated regions (UTR) are represented as rectangles with diagonal stripes and number 1, whereas open reading frames (ORFs) are shown as magenta, shaded cylinders that are numbered progressively from the 5' to the 3'. Small, white numbers outside the boxes and cylinders represent the number of amino acids encoded. Below the exon structure, the domain architecture of the protein product is shown, with the secondary structure elements included in the Longin Domain – α-helices as cylinders and β-strands as arrows. **(b)** Exon structure of the SYBL1b splice variant shown with the same convention as above. A frameshift results into a new, longer 3' in the mRNA that is shown as cyan shaded cylinders. The segmented white line represents the site of splicing. **(c)** Exon structure of the SYBL1c splice variant shown with the same convention as above. En exon skipping removes part of exon 2 and the whole exon 3.

VAMP7b is still uncharacterized, whereas VAMP7c has been shown lo lose the ability to bind AP3δ and be targeted to late endosomes [Martinez-Arca et al., 2003]. The SYBL1 splice system provides 2 "natural mutants" of LD and the SNARE motif, thus offering 2 powerful tools to investigate the biological relevance of "LD-SNARE coexistence" in longins in general, for which the advantage of coupling these two functionally independent elements together in one molecule is still far from being fully understood.

Only recently, Pryor and co-workers revealed that the ArfGAP Hrb directly mediates endocytosis of VAMP7 in Clathrin-coated vesicles [Pryor et al., 2008]. Strikingly, Hrb recruits VAMP7 by wrapping an unstructured C-terminal tail around the LD of VAMP7, in a fashion that is analogous to the coordination of the SNARE motif on to the LD of Ykt6 and Sec22b. In other words, a SNARE-like portion of Hrb behaves like the SNARE motifs of Ykt6 and Sec22b, showing the ability to bind the α1-β3 surface of the LD of VAMP7 (see **figure 6**). The VAMP7 SNARE motif competes for this binding, but direct biophysical data on a LD-SNARE interaction in VAMP7 are lacking

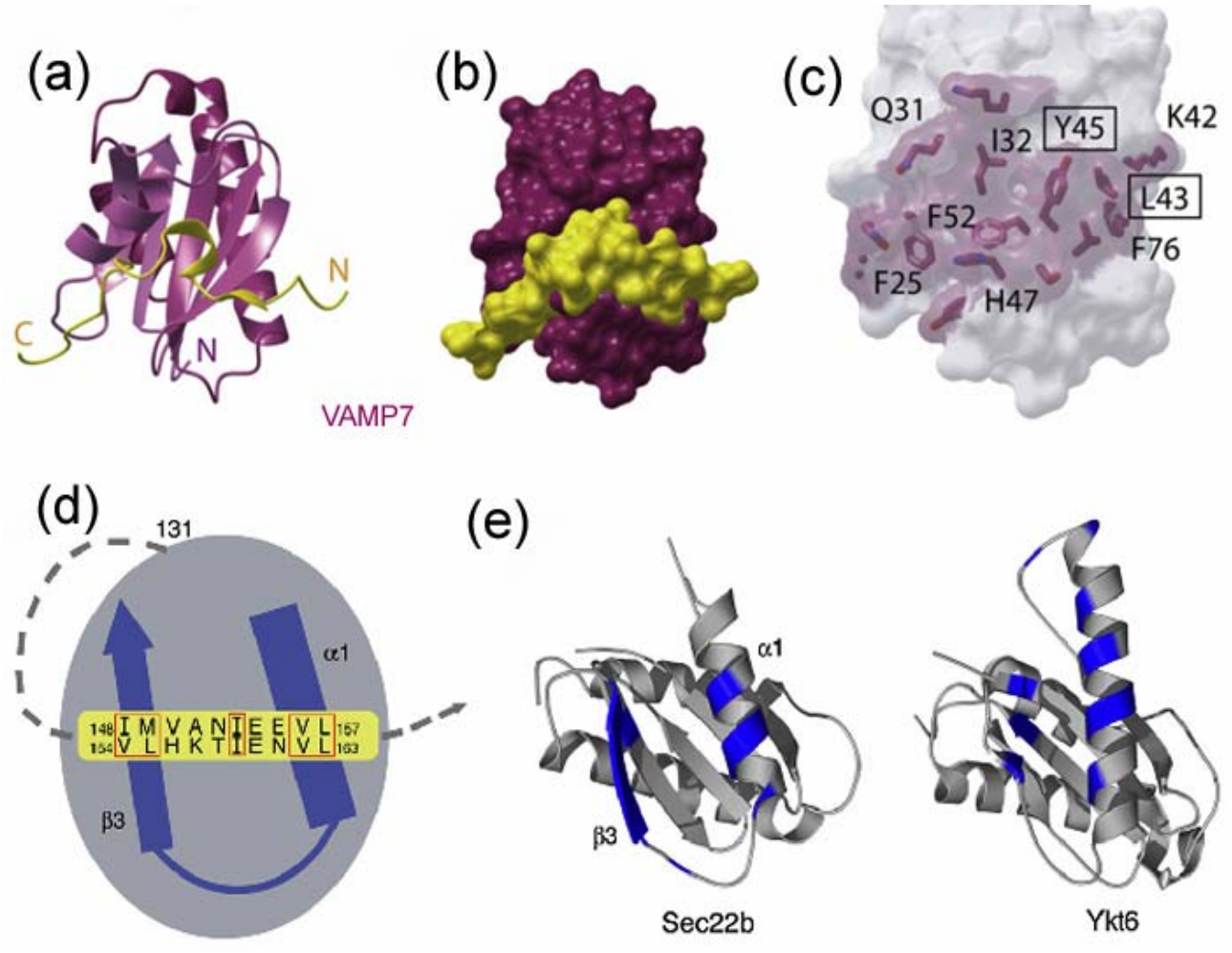

Figure 6. Interaction of the LD with Hrb and with the SNARE motif. **(a)** Ribbon representation of the complex between the LD in purple and the portion of Hrb(136-176) in gold, that is visible in the crystal structure. **(b)** Same as (a), but with a surface representation. **(c)** LD side chains involved in binding to Hrb and coloured in purple on a white surface representation of the LD. **(d)** Schematic cartoon showing the LD (grey circle) and its two structural elements (α1-β3, blue) interacting with a portion of the SNARE motif (yellow box). The SNARE residues contributing most to such interaction are enclosed in red boxes. **(e)** Ribbon representation of the LDs of Sec22b and Ykt6 (grey) with the structural elements binding to the SNARE motif highlighted in blue

The aim of this study

Preface

This three-year long PhD project was supported by a "PRIN" grant (from Italian Ministry for University and Research - MIUR) to Francesco Filippini (PhD tutor), by a "Cofin" additional support from the University of Padua and by Howard Hughes Medical Institute (HMMI) funding to Axel T. Brunger (collaborating research unit of Stanford University).

Scientific background of Padua and other collaborating research units

Longins and LDs were first identified and defined in our lab [Filippini et al., 2001] in collaboration with the groups headed by Maurizio D'Esposito (CNR-IGB, Naples) – who first discoveried SYBL1 [D'Esposito et al., 1996] – and by Thierry Galli (INSERM, Paris), who contributed to the characterization of its protein product TI-VAMP/VAMP7 [Galli et al., 1998; Martinez-Arca et al., 2000 and 2001]. This revealed a dual role played by the VAMP7 LD in regulating both membrane fusion and mediating subcellular localization [Martinez-Arca et al., 2003]. We further demonstrated that longins, rather than synaptobrevins, are the prototypical R-SNAREs [Rossi et al., 2004b]. This contributed a first work on longins evolution, that will be better addressed soon in collaboration with Joel B Dacks (University of Alberta, Canada) [Vedovato et al., in preparation]. We also show that alternative splicing of SYBL1 and other longins results in several VAMP7 variants characterized by different expression patterns and subcellular localizations [Vacca et al., in preparation]. Moreover, two-hybrid analysis of prototypical longins from different organisms were performed in our lab (V. Rossi, unpublished results), in collaboration with Dave K Banfield (Hong Kong University), who first demonstrated the LD-SNARE motif interaction [Tochio et al., 2001]. These analyses demonstrated an overall conservation of the LD-SNARE interaction amongst longins and organism evolution.

LDs and SNARE motifs have been directly related to neuronal diseases, as presented above. VAMP7 in particular seems to be a good model in this sense, not only for its direct linkage to neuronal plasticity and for its potential involvement in bipolar disorder, but also for the domain architecture of its main splice variants , which offer a chance to characterize natural variants of the classic LD-SNARE domain arrangement of longins.

The PhD research project

The lack of biophysical, direct data on the LD-SNARE interaction in VAMP7 gives us the opportunity not only to "fill some blanks" but also to provide and reveal new features of this

important mechanism. In fact, very little is known so far other than its distribution among longins and its mainly hydrophobic nature. We don't know for example if this happens to be a dynamic interaction resulting into a continuous fluctuation between an "open" and a "closed" conformation of the molecule or if it's rather a static coordination keeping the molecule in a closed, stable state. In other words, we don't know if longins distribute between two populations of molecules with either open or close LD-SNARE conformations, or if they instead group in a single population of closed molecules. Finally, we don't know if these dynamic properties are homogeneous along the SNARE motif or if there is certain diversity with eventual biological relevance. We lack any type of dynamic information on this mechanism. Gaining this knowledge would also allow us to acquire a comparative perspective on the analogies between LD-SNARE and Habc-SNARE interactions. The Habc-SNARE interaction of Syntaxins is in fact characterized to a larger extent than the LD-SNARE and the time is mature to confront the two mechanisms.

Taking advantage of the scientific background of the two laboratories where this research is performed and using VAMP7 as a model system, we aimed at shedding light on the biological relevance of the coexistence of LD and SNARE motif. In particular, in Axel Brunger's lab I investigated the presence of an intramolecular LD-SNARE interaction and performed characterization by biophysical methods, including multi angle laser light scattering (MALLS), X-ray crystallography and above all NMR spectroscopy. Finally, as we learnt from the example of Sec22b [Mancias and Goldberg, 2007], the intramolecular LD-SNARE interaction is not necessarily independent and functionally separated from intermolecular interactions with other key regulators of membrane traffic. Therefore, we look forward to determine in the future whether the LD-SNARE interaction can interfere and regulate the ability of VAMP7 to interplay with other key player of membrane fusion.

Materials and methods

DNA constructs

Using standard PCR techniques and VAMP7 templates provided by Prof. Filippini (Padova research unit), we cloned a panel of cDNA constructs that are shown in **table M1**.

E. coli TOP 10 cells (invitrogen) were used as hosts for the recombinant cDNA vectors. The restriction enzymes used were purchased from New England Biolabobs and used according to manufacturer's instructions.

cDNA	Express. Vector	Restrict. sites	Fusion partner	Purif. tag	Express. Temp.(°C)
Vamp7a(1-118)	pET32H	NcoI-BamHI	Thioredoxin	His_6	29
	pET47b	XmaI-XhoI	-	His_6	29
	pGEX-6P1	BamHI-XhoI	GST	GST	29
Vamp7a(1-121)	pET32H	NcoI-BamHI	Thioredoxin	His_6	15,29,37
	pET47b	XmaI-XhoI	-	His_6	29
Vamp7a(1-149)	pET32H	NcoI-BamHI	Thioredoxin	His_6	29
	pET47b	XmaI-XhoI	-	His_6	29
Vamp7a(1-150)	pET32H	NcoI-BamHI	Thioredoxin	His_6	29
	pET47b	XmaI-XhoI	-	His_6	29
Vamp7b(1-150)	pET47b	XmaI-XhoI	-	His_6	29
Vamp7b(119-260)	pET32H	NcoI-BamHI	Thioredoxin	His_6	15,29,37
Vamp7c(1-80)	pET32H	NcoI-BamHI	Thioredoxin	His_6	15,29,37,42
	pGEX-6P1	BamHI-XhoI	GST	GST	29
Vamp7c(1-146)	pET32H	NcoI-BamHI	Thioredoxin	His_6	29

Table 1. Summary of Cloning and expression of VAMP7 cDNAs in *E.coli*. The table reports (from left to right): (i) the recombinant cDNAs encoding the proteins of interest; (ii) the expression vector used; (iii) the restriction sites in used for cloning (iv) the fusion partner and (v) the purification tag encoded by the expression vector; (v) the temperature at which the expression was performed.

Cell cultures and protein expression

E. coli cells BL21 (DE3) (Invitrogen) were grown at 37°C in Terrific Broth - II (MP Biomedicals) medium containing either 100 μg/ml ampicillin for the expression of pET32-based constructs or 50 μg/ml kanamicyn for the expression of pET47b-based constructs. Protein expression was induced at OD_{600}=1 with 0.15 mM IPTG and was carried for 3-4 hours at 29°C. Cell were finally harvested, washed in PBS, frozen in liquid nitrogen and stored at -80°C for future use.

protein purification

From pET32H expression vectors

Frozen cell pellets were resuspended in lysis buffer (1/20 or 1/40 of the colture volume) containing 50 mM Tris-HCl, pH 7.0-8.2 (difference with the pI of the recombinant was maximized in this range), 500 mM NaCl, 10 mM Imidazole, 5 mM β-mercaptoethanol, one EDTA-free protease inhibitor tablet (Roche). Lysozime and DNAase were arbitrarily added in order to improve next cell lysis and sample viscosity respectively.

After 15' of equilibration (rotation) at 4°C, the fully resolubilized cells were lysed either by sonication or microfluidification. Sonication was performed on a Sonicator XL, CL4 tip (Misonix), by alternating 5"-long pulses with 5"-long pauses (5" ON - 5" OFF) resulting into a combined 3-4'-long pulse. Microfluidification was achieved by running the sample three times into on a Microfluidizer Processor M-110EH (Microfluidics) at 1800 psi (0.26 Pa). The cell lysates were ultracentrifuged at 150000 g (44000 rpm, Beckman Ti45 rotor) for 1 hour and the supernatant was retained as soluble fraction for the following steps. Affinity chromatography was adopted as the capture step. Nickel beads (Ni-NTA Superflow, QIAGEN) were added to the sample and incubated (1ml beads/5mg of protein) for 4 hours at 4°C (batch mode). The sample was washed with 50 mM Tris-Hcl pH 8.0, 500 mM NaCl, 5 mM β-mercaptoethanol, 30 mM imidazole (100 resin volumes). The recombinant protein was eluted in six fractions of 50 mM Tris-Hcl pH 8.0, 500 NaCl, 5 mM β-mercaptoethanol, 300 mM imidazole (1/3 resin volume for the first fraction and 1 resin volume for the following 5). Over night dialyses were used to change the buffer to 50 mM Tris-HCl pH 8.0, 200 NaCl, 5 mM β-mercaptoethanol. This composition was varied in order to avoid the formation of aggregates observed during the dialysis.

The removal of the N-ter partner fusion from the recombinant protein was achieved by an overnight

reaction with Thrombin (bovine α-thrombin, Haematologic Technologies, Inc) at 4°C following manufacturer's instructions. Another affinity chromatography with Ni^{2+} beads was used to separate the recombinant protein from the His6-containing fusion partner. In fact, the flow-through was collected after batch binding. This step was repeated two times to better remove the fusion partner contaminant. The final polishing was accomplished by gel-filtration (GF) chromatography (ÄKTA, GE Healthcare) using Superdex 75 columns: HR 10/30 for analytical purposes and HiLoad 16/60 for large-scale preparation (GE Healthcare). The elution was performed in 20 mM Tris-HCl, 100 NaCl, 1 mM DTT. 1 mM TCEP was added afterwards before storing the sample at 4°C.
The purification process was monitored by SDS-PAGE and Coomassie Brilliant Blue staining.

From pET47b expression vectors

Purification of recombinant proteins expressed from pET47b vectors were performed as the ones from pET32H, but with the following differences: (i) 0.2% X-Triton and 0.2% Tween-20 were added to the lysis buffer. The Thrombin cleavage was replace by a Prescission protease (GE Healthcare) over night proteolysis reaction at 4°C. This was followed by a final GF only, as no fusion partner removal was needed.

Mass spectrometry

Mass spectrometry experiments were performed with the Matrix-assisted laser desorption/ionization (MALDI) technique on a Omniflex high vacuum MALDI-TOF (time-of-flight) mass spectrometer (Bruker Daltonics). Pure protein samples were further concentrated and purified using C18 ZipTips (Millipore) according to the manufacturer's recommendations and eluted directly onto the MALDI plate using sinapinic acid in 50% acetonitrile as the matrix.

Circular dichroism

CD data were collected on an Aviv 202–01 spectrometer using a 1-mm-path length cell. Protein samples were 50 μM in buffer containing 20mM sodium phosphate, pH 6.5, 100mM NaCl, 1 mM DTT. Protein concentrations were determined by UV spectrophotometry at 280 nm and BCA assay (Pierce). The experiment scanned wavelengths from 190 to 260 nm, with increments of 1nm, avering time of 1 sec and settling time of 0.33 sec.

light scattering

from [Ernst-Brunger 2003]: Multi-angle Laser Light Scattering (MALLS)—Size exclusion chromatography was performed using a Superdex 200 10/30 column at a flow rate of 0.5 ml/min. Measurements were performed in 150 mM NaCl, 10 mM HEPES, pH 7.8, and 5 mM DTT. The elution profile was monitored by UV absorption at 280 nm, light scattering at 690 nm, and differential refractometry. Light scattering and differential refractometry were carried out using the Dawn and OptiLab instruments (Wyatt Technology). Analysis was carried out using the Astra software (22). For each sample, 100 _l of protein at 1 mg/ml protein was loaded. The differential refractive index increment (dn/dc) is fairly constant for globular proteins and was set to 0.185 units.

Crystallization trials

Pure recombinant VAMP7a(1-118), VAMP7a(1-121), VAMP7a(1-149) and VAMP7a(1-150) were concentrated by using Amicon© centrifugal filter devices (Millipore). Different concentrations of protein – ranging from 6 to 15 mg/ml – were used to set up crystallization trays on either 96 well INTELLI-PLATE (Art Robbin Instruments) or 24 well EasyXtal tool (QIAGEN), adopting the sitting and hanging drop method respectively. The 96 trays were set up using customized or pre-made screening conditions. These latter were:

- EasyXtal MPD Suite (QIAGEN)
- EasyXtal PEGs Suite (QIAGEN)
- EasyXtal PEGs II Suite (QIAGEN)
- EasyXtal AmSO4 Suite (QIAGEN)
- SaltRx (Hampton Research)
- Crystal Screen HT (Hampton Research)
- Index (Hampton Research)

All the 96 well-trays were set up using the automated Phoenix Liquid Handling System and the Phoenix 1.9 dedicated software (Art Robbin Instruments). Sitting drops (600 nl) contained a 1:1 (v/v) ratio of protein to reservoir solution. Reservoir solution was set to 90 µl. 24 well-trays were set up manually. Hanging drops (1 µl) contained a 1:1 (v/v) ratio of protein to reservoir solution (500 µl).

Nuclear Magnetic Resonance

Uniform ^{15}N and ^{13}C labelling in two combinations (only ^{15}N label or both ^{15}N and ^{13}C) was accomplished by growing *E coli* BL21 (DE3) in M9 minimal media with $^{15}NH_4Cl$ and $^{13}C_6$-labeled glucose as the sole nitrogen and carbon sources, respectively. All samples were prepared in 20 mM potassium phosphate buffer (pH 6.5) containing 100 mM NaCl and 1 mM DTT, unless otherwise indicated, using H_2O:D_2O 90:10 (v/v). The protein concentrations were 150–400 μM for ^{1}H-^{15}N HSQC experiments of VAMP7a(1-118), VAMP7a(1-150), VAMP7b(1-150), and 450 μM for the ^{1}H-^{15}N-^{13}C 3D experiments used for resonance assignment of VAMP7a(1-118). These experiments were performed using standard sensitivity-enhanced, pulsed-field gradient-based pulse sequences for double and triple resonance spectra [Zhang et al. 1994] and included: 3D ^{1}H-^{15}N NOESY-HSQC, HNCACB, CBCA(CO)NH, C(CO)NH all acquired on the uniformly ^{15}N, ^{13}C-labeled sample.

All resonance assignment data were acquired on a 600 MHz Varian ^{UNITY}INOVA at 10°C. The other ^{1}H-^{15}N HSQC experiments were acquire on either the 600 or an 800 MHz Varian ^{UNITY}INOVA at 25°C. Both instruments are equipped with 5 mm, H{CN} triple resonance, gradient probes. All the data were acquired using the VNMR software (Varian, Inc.) and analyzed with Sparky [T. D. Goddard and D. G. Kneller, SPARKY 3, University of California, San Francisco].

Results and discussion

Domain architecture variations of VAMP7b and VAMP7c impairs protein stability in *E. coli*

The SYBL1 gene is regulated by alternative splicing and encodes a main variant – VAMP7a – other than two minor ones, simply termed b and c. These three variants comprise a model system to study the outcome of variations in the LD or the SNARE motif. In fact, VAMP7b includes a variation in the C-terminal half of the SNARE domain that creates a longer C-terminus region of unknown function, whereas VAMP7c lacks 41 amino acids in the core of the LD sequence (see Introduction).
In order to characterize these proteins, we cloned and expressed a number of recombinant fragments of the variants "b" and "c", as shown in **figures R1 and R2** (see also Materials and Methods).
Expression temperatures and fusion partner were varied and tested in order to try and improve recombinant protein expression and solubility: (i) four different expression temperatures from 15 to 42 °C, with the 15°C expression performed over night and the others completed within 3-4 hours; (ii) two different fusion partners, Thioredoxin and GST.
In spite of these variations the results were consistent. Expression of VAMP7b-specific C-terminal region could not be detected (see **figure R2b**). Both the VAMP7c-specific N-terminal region and the fragment N-terminal to the transmembrane domain could be expressed. However the full length recombinant proteins proved insoluble and prone to degradation in *E. coli*, as only truncations comprising the fusion partner could be purified under native conditions (see **Figure R2c**). This data collectively suggest a strong decrease of protein stability in *E. coli* resulting from the variations of the SNARE and longin domains in VAMP7b and VAMP7c. This instability may be directly caused by the structural rearrangements *per se* of the two domains. We cannot also exclude that these proteins eventually require post-translational modifications, specific co-factors or molecular interactors that cannot be found in a prokaryotic system. Expression in a eukaryotic system may provide an answer to these questions.

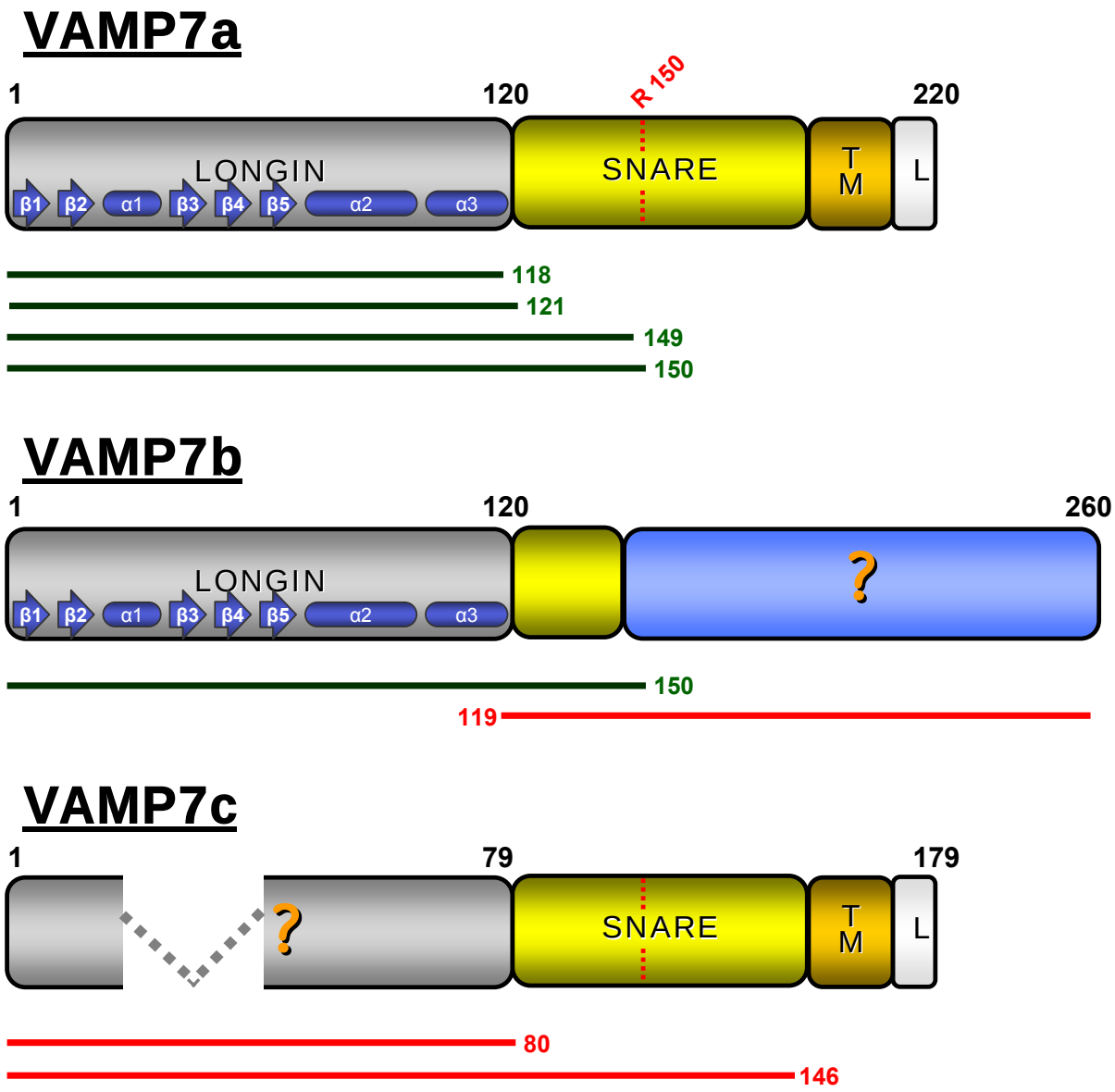

Figure R1. Graphic summary of the recombinant proteins expressed in E. coli to characterize the VAMP7 splice variants. The domain architecture of the three variants VAMP7a/b/c is shown with shaded boxes: the LD in grey with its secondary structural elements in dark blue (arrows for β-strands and cylinders for α-helices), the SNARE domain in yellow with its ionic layer signed as red dashed line, the transmembrane domain (TM) in orange and finally the short luminal (L) tail in white. Numbers represent positions in the amino acid sequences. A cyan box and a grey, segmented one represent the variant regions of VAMP7b and VAMP7c, respectively. Their unknown biochemical features are symbolized by orange question marks. Dark green or red lines stand for the recombinant fragments expressed in E.coli for each of the VAMP7 variant. Dark green corresponds to a successful expression and purification leading to a pure soluble protein, whereas red signifies an expression failure.

(a)

cDNA	Express. Vector	Fusion partner	Purif. tag	Express. Temp.(°C)	Express. results
Vamp7b(1-150)	pET47b	-	His_6	29	✓Positive
Vamp7b(119-260)	pET32H	Thioredoxin	His_6	15,29,37	✓Negative
Vamp7c(1-80)	pET32H	Thioredoxin	His_6	15,29,37,42	✓Negative
	pGEX-6P1	GST	GST	29	✓Negative
Vamp7c(1-146)	pET32H	Thioredoxin	His_6	29	✓Negative

(b)

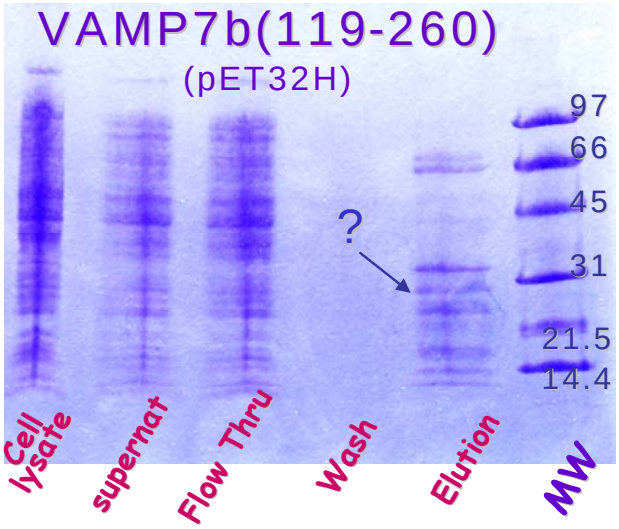

(c)

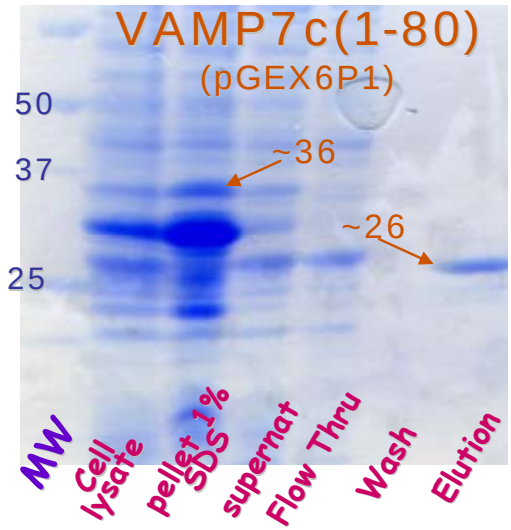

Figure R2. VAMP7b and VAMP7c expression trials at 37°C. **(a)** An extract of table M1 summarizes the recombinant fragments of VAMP7b/c tested in expression trials and the correspondent expression parameters (see table M1 legend). **(b)** The attempt to express VAMP7b(119-260) cloned in the pET32H vector and purify a recombinant Thioredoxin-VAMP7b(119-260) fusion protein in native conditions is monitored by a 8-25% acrylamide SDS-PAGE (comassie staining). Lanes content (from left to right): (i) sonicated *E. coli* cell lysate; (ii) clear cell lysate; (iii) flow through; (iv) wash and (v) elution of a Ni-NTA (Qiagen) affinity chromatography; (vi) Low Range protein standards (Biorad). The blue question mark symbolizes the inability to detect any band, clearly related to the full length (~30 KDa) protein of interest. **(c)** The attempt to express VAMP7c(1-80) cloned in the pGEX-6P1 vector and purify a recombinant GST-VAMP7c(1-80) fusion protein in native conditions is monitored by a 12.5% acrylamide SDS-PAGE (comassie staining). Numbers represent molecular weights (KDa). The lanes report (from left to right): (i) Precision Plus protein standards (Biorad); (ii) sonicated *E. coli* cell lysate (iii); cell lysate pellets resolubilized by sonication in 1%SDS (denaturing condition) (iv) clear cell lysate (ultracentrifugation supernatant); (v) flow through, (vi) wash (vii) and elution of a Ni-NTA (Qiagen) affinity chromatography. A full length (36 KDa) recombinant GST-VAMP7c(1-80) is visible in (iii). Only a truncated fragment of about 26 Kda can be purified under native condition.

LD-SNARE interaction in VAMP7a

Design of VAMP7a recombinant proteins

In order to study the coexistence of LD and SNARE domain in VAMP7a and to assess the presence of intramolecular interactions, we designed cDNA constructs encoding different truncations of the VAMP7a protein (see Materials and Methods). The choice of the length of these truncations was based on the information available in the literature about LD-SNARE interactions in Ykt6 and Sec22b [Tochio et al., 2001; Mancias et al., 2007]. In particular, a sequence homology comparison helped us identify a SNARE fragment, i.e. VAMP7a(139-148) potentially acting as a binding target for the LD, as shown in **figure R3a**.

Our experiments focused on two truncations of VAMP7, one consisting of the LD and the other consisting of a longer recombinant protein including the putative LD-binding site in the SNARE motif. Hereafter, We will refer to these two samples as "LD" and "LD+SNARE" for simplicity. Each of the two versions was actually produced in two minor variants in order to test optimal sample solubility and behaviour *in vitro*. Precisely, this resulted into using the following four recombinant proteins: VAMP7a(1-118), VAMP7a(1-121), VAMP7a(1-149) and VAMP7a(1-150) (see **figure R3b**).

Biochemical and Biophysical characterization of VAMP7 truncations

Four truncations of VAMP7a were expressed as recombinant proteins in *E. coli* with an N-terminal hexahistidine tag and with or without Thioredoxin as an additional N-terminal fusion partner (see Materials and Methods). The Thioredoxin-conjugated proteins were easily over expressed and yielded soluble proteins in native conditions from *E. coli* cell lysates. However, to remove the fusion partner – with a molecular mass comparable to VAMP7a fragments – required many purification steps resulting in final low yields. Therefore, we switched to Thioredoxin-free constructs and included detergent in the early steps of protein purification, in order to compensate the reduced solubility of the recombinant proteins and maximize purification yields. In fact, expression without a fusion partner and extraction without any detergent results in very little amounts of soluble LD. Addition of detergent in the early steps of the purification process does not cause denaturation of the LD as shown by circular dichroism (CD) spectroscopy (figure R4).

Moreover, it helped prevent oligomerization and aggregation as shown by the improvement of gel filtration elution profiles (**figure R5**).

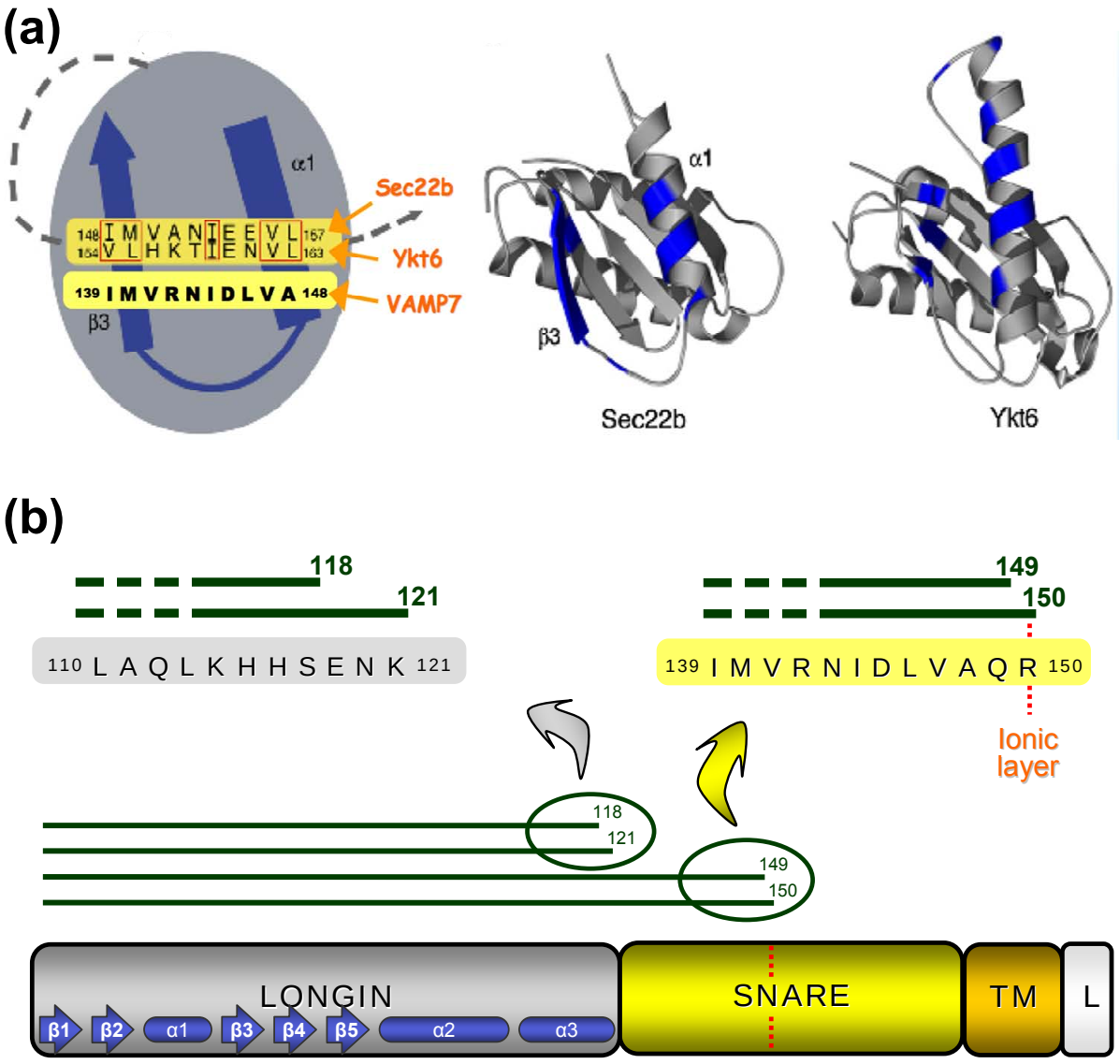

Figure R3. (a) Sequence similarity-based identification of a putative LD-binding site on the SNARE motif of VAMP7. The LD-SNARE interaction of Ykt6 and Sec22b is schematically shown as in figure R1. The putative LD-binding region of the SNARE motif is added as yellow box aligned below the one comprising the Ykt6 and Sec22b amino acid sequence. **(b)** From bottom up: the domain architecture of VAMP7 is shown with shaded boxes: the LD in grey with its secondary structural elements in blue (arrows for β-strands and cylinders for α-helices), the SNARE domain yellow with its ionic layer signed as red dashed line, the transmembrane domain in orange and finally the short luminal tail in white. The four VAMP7 truncations used are shown as dark green lines. A close-up view of their C-termini is shown along with the amino acid sequence in boxes coloured with the same colour code as below.

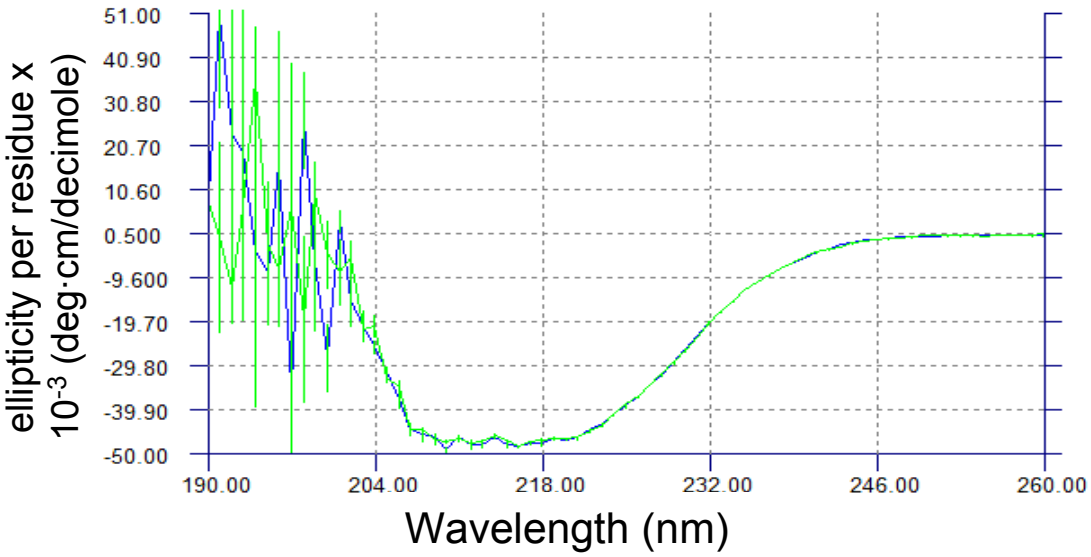

Figure R4. Circular dichroism spectrum (blue profile) of VAMP7 LD (error bars in green) in the far UV region. The spectrum profile is typical of a protein folded into a well-defined structure. The positive signals at wavelengths greater than 250 nm, the minimum at 220 nm and the absence of strongly negative values around 194 nm support little random coil in VAMP7 native LD fold.

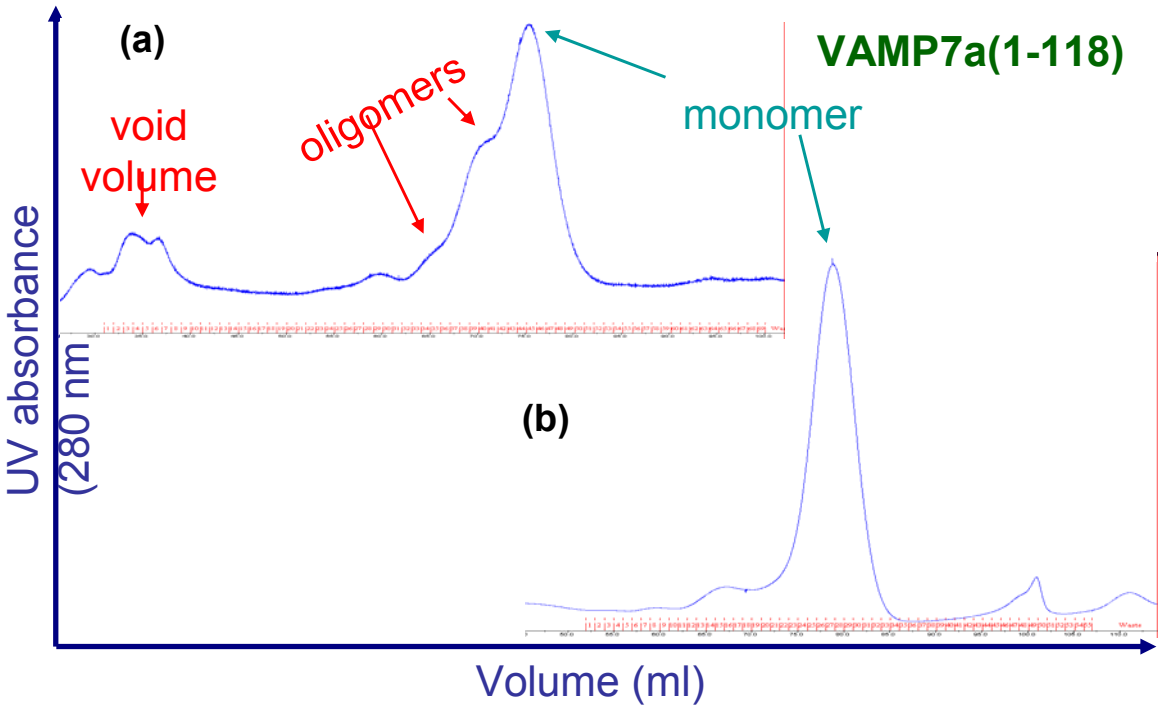

Figure R5. Gel Filtration elution profiles of VAMP7a(1-118) monitored by UV light absorbance at 280 nm over column volume .**(a)** VAMP7 LD that has been expressed without any fusion partner, extracted without any detergent and then purified by affinity chromatography shows oligomeric states in solution (peaks pointed by red arrows) and some aggregation ("void volume"). **(b)** VAMP7 LD that has been expressed without fusion partner, but then extracted with the addition of low percentages of detergent and purified by chromatography affinity shows a homogeneous monomeric state in solution.

Further, the smaller number of purification steps allowed us to halve the time cost and increase pure protein yields from roughly 1 to 6 mg per 1L of *E. coli* BL21 culture (see Materials and Methods). All VAMP7 truncations could be purified in their full extension without observing any degradation, as shown by the exact molecular weights measured by mass spectrometry (**figure R6**).

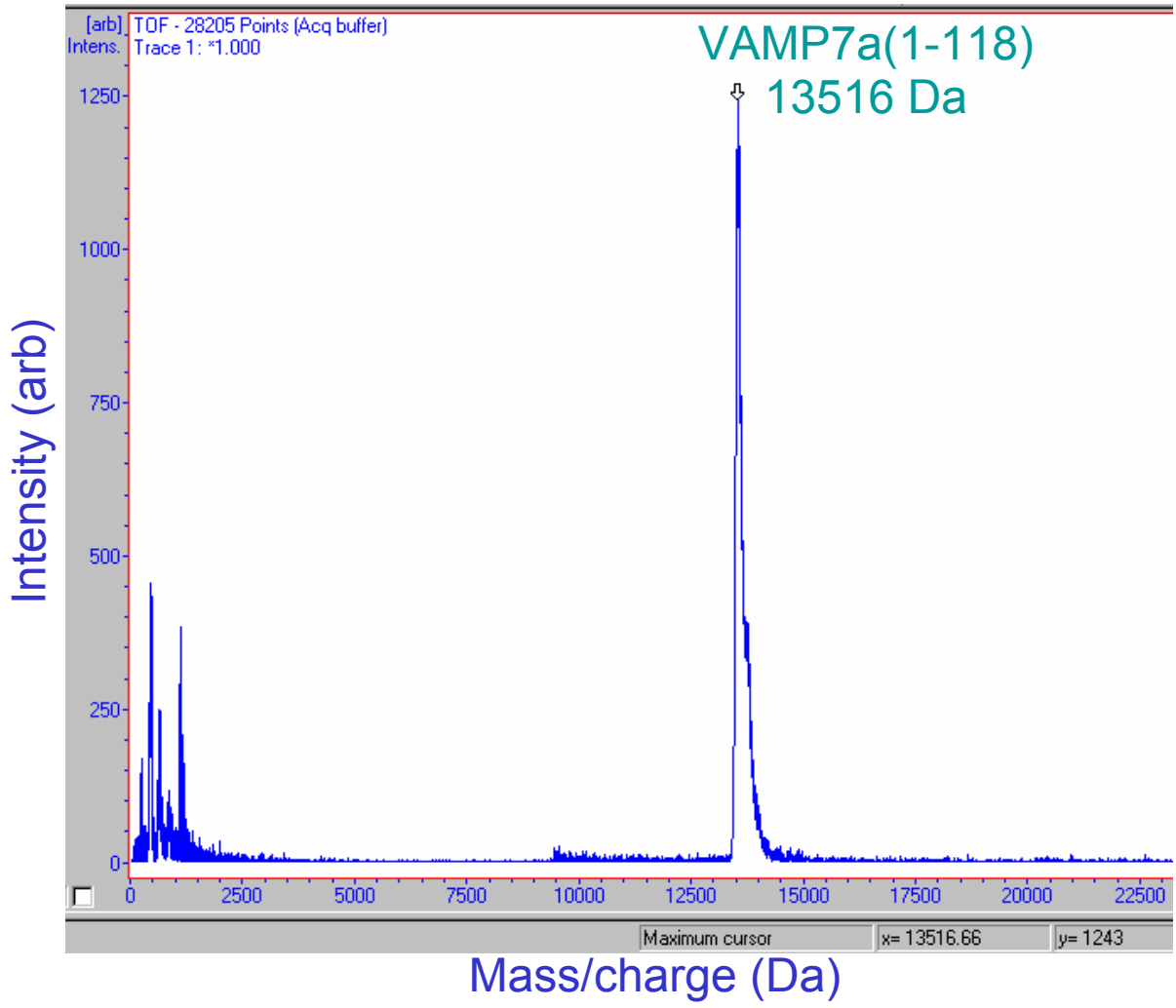

Figure R6. Mass spectrum of a pure VAMP7 LD (VAMP7a(1-118)). The experimental valiue (13.5 kDa) corresponds to the theoretical one for VAMP7a(1-118). No other signals are evident in the spectrum, indicating high purity of the sample and absence of degraded species.

Irrespective of the protein preparation protocols used, we observed different behaviours for the different VAMP7a truncations in solution. The LD – either VAMP7a(1-118) or VAMP7a(1-121) – shows a concentration-dependent tendency to aggregate, as white pellets visibly appear when concentrating pure protein from the µM to the mM range in low ionic strength – structural studies require milligrams of proteins in highly concentrated samples. Aggregates occur over time as well.

In contrast, LD+SNARE – VAMP7(1-149) and especially VAMP7(1-150) – shows higher expression levels in *E. coli* and no tendency to aggregate, as protein concentrations greater than 10 mg/ml were achieved with little or no particulates forming.

These qualitative observations were confirmed by studying the oligomeric state of LD and LD+SNARE in solution by Size Exclusion Chromatography-Multi-angle Laser Light Scattering (SEC-MALLS). Pure monomeric samples of VAMP7a(1-121) and VAMP7a(1-149) were purified by size exclusion in low ionic strength (150 mM NaCl), concentrated to 3 mg/ml and left to equilibrate over night. Following this, they were analysed by SEC-MALLS: the new size exclusion elution profile, combined with the light scattering at 690 nm showed an equilibrium between monomeric and dimeric species for VAMP7a(1-121) and a homogeneous monomeric state for VAMP7a(1-149) (**figure R7**). The same experiment repeated at medium ionic strength (250 mM NaCl) and in the presence of 5% glycerol showed only monomeric states for both VAMP7a(1-121) and VAMP7a(1-149) (**figure R8**).

These results suggest a weak intermolecular LD-LD interaction resulting into partial LD dimerization that can be disrupted at medium salinity and that may be the starting point of the aggregation process. In contrast, the presence of the SNARE fragment at the C-terminus of the LD is enough to prevent this association, maintaining the molecule completely monomeric. This could be a first suggestion about a possible role of the SNARE motif in “shielding” a surface of the LD where the dimerization occurs.

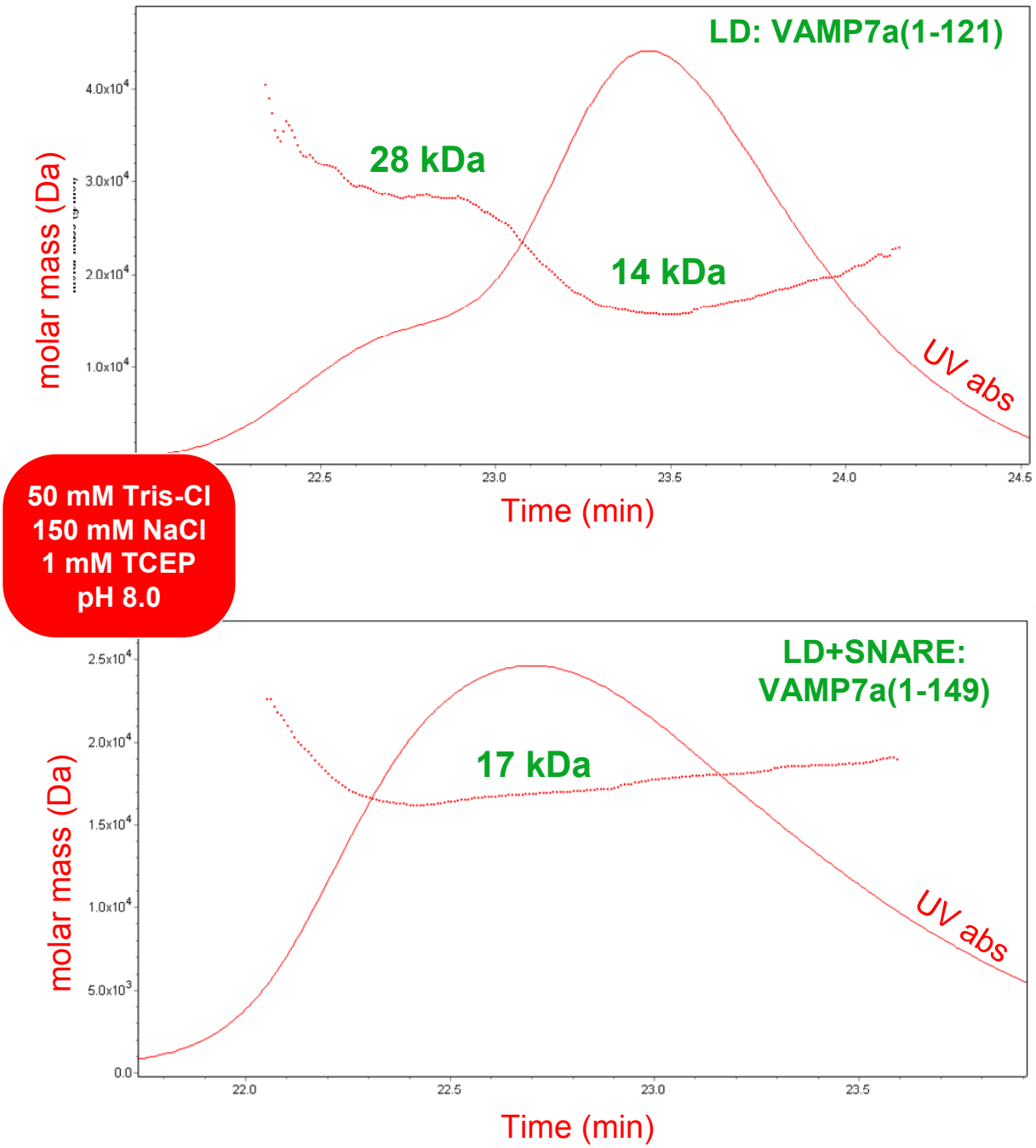

Figure R7. Size Exclusion Chromatography-Multi-angle Laser Light Scattering (SEC-MALLS) data of VAMP7a(1-121) and VAMP7(1-149) in low ionic strength (buffer conditions in red box). SEC is monitored by UV light absorbance profile, reported together with the calculated molecular weight (or molar mass). The LD (upper spectrum) shows a monomer-dimer equilibrium, whereas the LD+SNARE is purely monomeric.

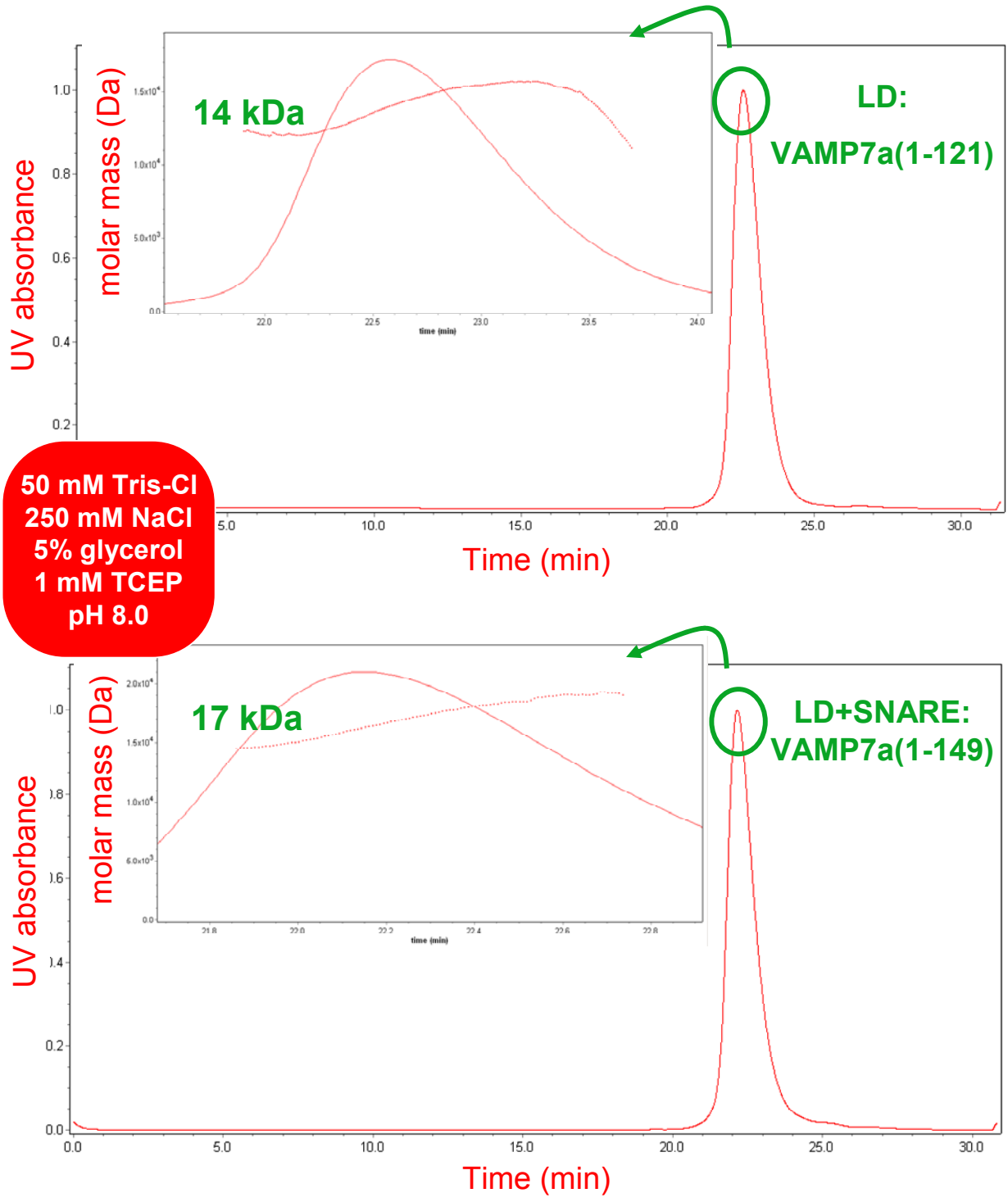

Figure R8. Size Exclusion Chromatography-Multi-angle Laser Light Scattering (SEC-MALLS) data of VAMP7a(1-121) and VAMP7(1-149) in medium ionic strength and 5% glycerol. The figure convention is the same as with figure R5, with the difference that the complete, larger SEC profiles are also shown behind the close up views of their peaks. Both LD and LD+SNARE are purely monomeric in these conditions.

Targeting LD-SNARE interaction by X-ray crystallography

We chose X-ray crystallography as the first approach to learn high resolution information from the VAMP7 LD structure and its eventual interaction with the SNARE motif. The X-ray structures of the LD and of the LD+SNARE truncations of VAMP7 would give the chance to observe an eventual interaction of the SNARE fragment onto the LD and also to highlight fine structural LD rearrangements due to such interaction.

Therefore, crystallization trials were undertaken for all the 4 different VAMP7 truncations, as slight differences in the chemical-physical properties of a molecule often have a great impact in its tendency to form crystals. Taking advantage of the automated "Phoenix Liquid Handling System" and of the many commercially available crystallization screens, we were able to set up roughly 1-5 thousand sitting drop crystallization trials for each of the four VAMP7 truncations. The different conditions explored variations of some critical factors, such as (i) the protein concentration and (ii) the buffer composition of the pure protein sample, as well as the type of (iii) precipitant agent and (iv) additives of the sitting drop system, and finally (v) the temperature of the experiment. The LD formed crystals very easily within 3-5 days with ammonium sulfate (from 1.6 to 3.2 M), often combined with poly ethylene glycol (PEG) – no particular additives are favoured. These crystals grew in clusters with overall dimensions in the order of hundreds of μm in many cases. By eye, these clusters are made of either long needles or flat plates. Figure R9 reports some examples along with the exact crystallization conditions. The presence of ammonium sulfate and PEG and the preference for slightly acidic pHs make our crystallization conditions consistent with those of the Sec22b LD [Gonzalez et al., 2001]. This evidence, together with the relatively small dimensions, suggested the crystals were actually made of protein rather than salt. However, in order to confirm this hypothesis, we broke one of these clusters with a micro cutter, isolated a single plate and tested it at the Stanford synchrotron radiation laboratory (**figure R9b**). The X-ray diffraction was limited by poor resolution (~9 Å) obtained in the direction were the plate was thinnest, whereas the orthogonal direction yields coherent Bragg scattering to ~3.5 Å. Despite the law quality diffraction, the high number of spots and their d-spacing indicated a large crystal lattice made up of protein.

A possible explanation for not obtaining good three-dimensional crystals may reside in the fact that crystal-packing protein-protein contacts are strongly favoured in one direction over the others, resulting in a high crystal grow rate in only one or two dimensions. This would be consistent with what observed for Sec22b, whose isolated LD crystallized as a fibre formed by donor-acceptor interactions of LDs running in only one direction (**figure R10**) [Gonzalez et al., 2001; Mancias and Goldberg 2007]. This may also be consistent with our light scattering data, showing the possibility

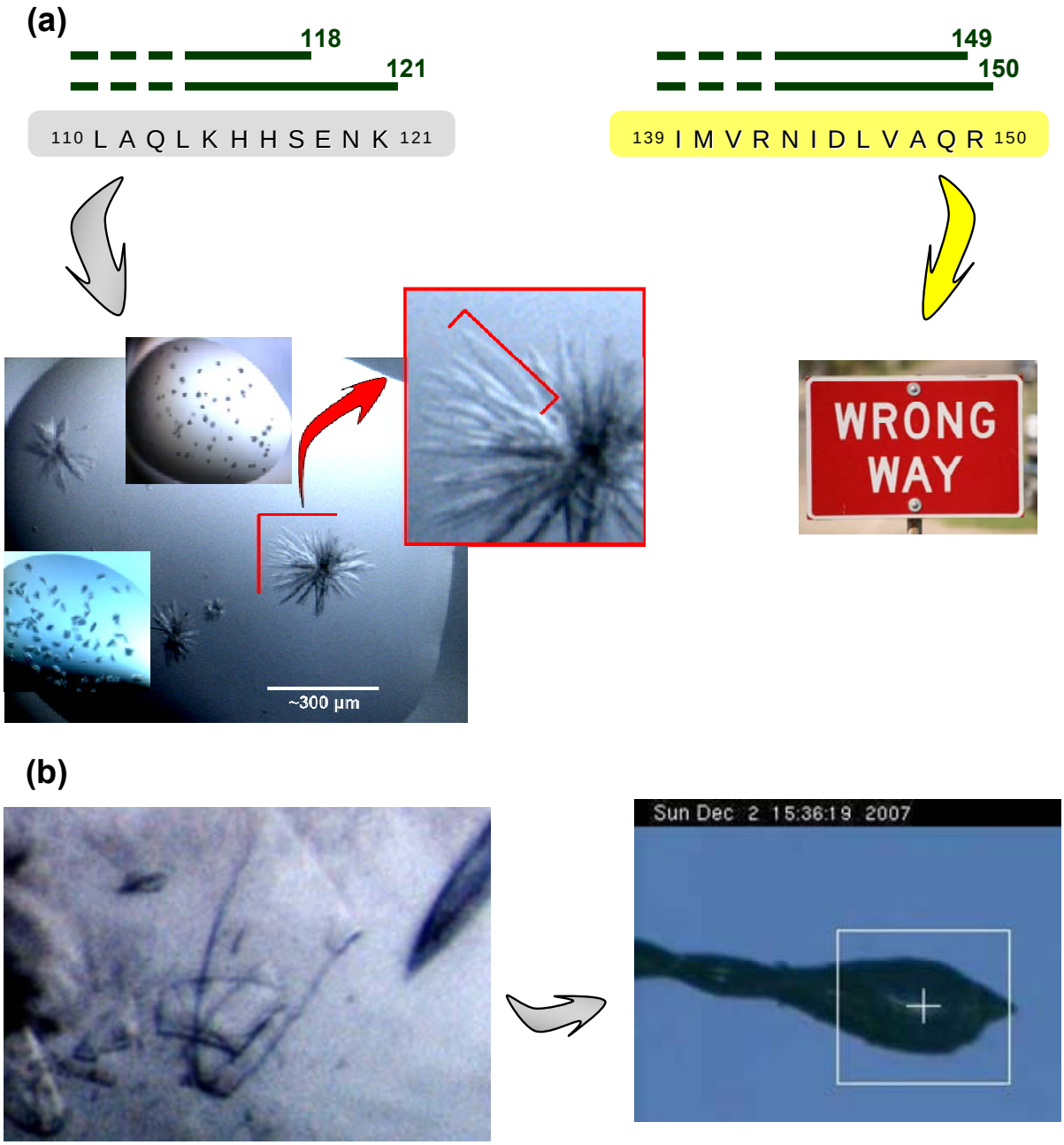

Figure 9. Outcome of the crystallization trials for the different VAMP7 truncations. **(a)** Left side: both the two truncations (same convention as in figure #) corresponding to the LD easily crystallize in clusters of multiple plates. A photograph of some of these clusters is shown down on the left, with a close up view (red square) of one of them: needle-shaped crystals obtained in 30% PEG 8000, 0.1 M Na Cacodylate pH 6.5, 0.2 M AmSO4. Right side: a wrong side road sign represents the inability of the two LD+SNARE truncations to form crystals. **(b)** A flat crystal plate, obtained in 0.2 M Ammonium bromide, 2.2 M Ammoium sulfate, is dissected from a cluster and tested at the Stanford Synchrotron Radiation Lightsource (SSRL).

Figure R10 (adapted from Mancias and Goldberg 2007). Backbone rapresentation of the crystal structure of the isolated Sec22b LD drawn in thick lines; five additional copies of LD are added to indicate the fibre formed by donor(blue ball)-acceptor(yellow ball) interactions that runs through the crystal in the direction of the crystallographic c axis.

for the LD to dimerize in solution. A way to overcome such problem in x-ray crystallography is known as surface engineering and consists in targeting mutagenesis of surface patches containing residues with large flexible side chains. Their replacement with smaller amino acids is likely to favour crystal packaging contacts. Using this technique on specific surfaces of interest, in order to increase the crystal rate of growth in one particular dimension, may lead to better three-dimensional crystal and ultimately to better diffraction quality [Derewenda 2004]. Another solution could be instead to screen different additives to couple to ammonium sulfate.

However, we did not test these solutions and we did not go further in our trials to achieve better LD crystals, because of the outcome of the LD+SNARE crystallization trials. In fact, the LD+SNARE truncations of VAMP7 didn't form any crystals in spite of the many crystallization conditions tested. It is reasonable to believe that the unstructured SNARE fragment may be flexible enough to affect crystal packing. Because of the inability to obtain crystals in our trial for the LD+SNARE and because of the likely dynamic nature of the SNARE fragment, we therefore switched to NMR spectroscopy to improve the likelihood of addressing the LD-SNARE interaction in a more informative way.

Discovery and characterization of LD-SNARE interaction by Nuclear Magnetic Resonance

In order to reveal an eventual LD-SNARE interaction in VAMP7a, we compared the $^{1}H\{^{15}N\}$-heteronuclear single-quantum coherence (HSQC) spectrum of the LD (VAMP7a(1-118)) to that of the LD+SNARE (VAMP7a(1-150)) – both proteins were uniformly ^{15}N-labelled. The LD (VAMP7a(1-118)) spectrum showed good dispersion of N-H resonances, which is indicative of the

heterogeneity of chemical environments that different amides experience in the LD. In other words, this is consistent with a native folding of the VAMP7 LD, as already anticipated by CD (see "Biochemical and Biophysical characterization of VAMP7 truncations"). Similar LD peaks are seen in the LD+SNARE (VAMP7a(1-150)) spectrum, confirming that LD adopts a similar fold in the LD+SNARE truncation. By contrast, the additional resonances attributed to the SNARE motif, mostly overlapping in the central region of the VAMP7a(1-150) spectrum, support that the SNARE adopts an unstructured, random-coil conformation. Other than these two basal observations, the comparison of the two spectra gives us important information: a number of chemical shifts of the LD vary their resonances in the presence of the SNARE motif. The change of chemical environment sensed by their nuclei is the first direct evidence of an LD-SNARE interaction in VAMP7a (**figure R11**).

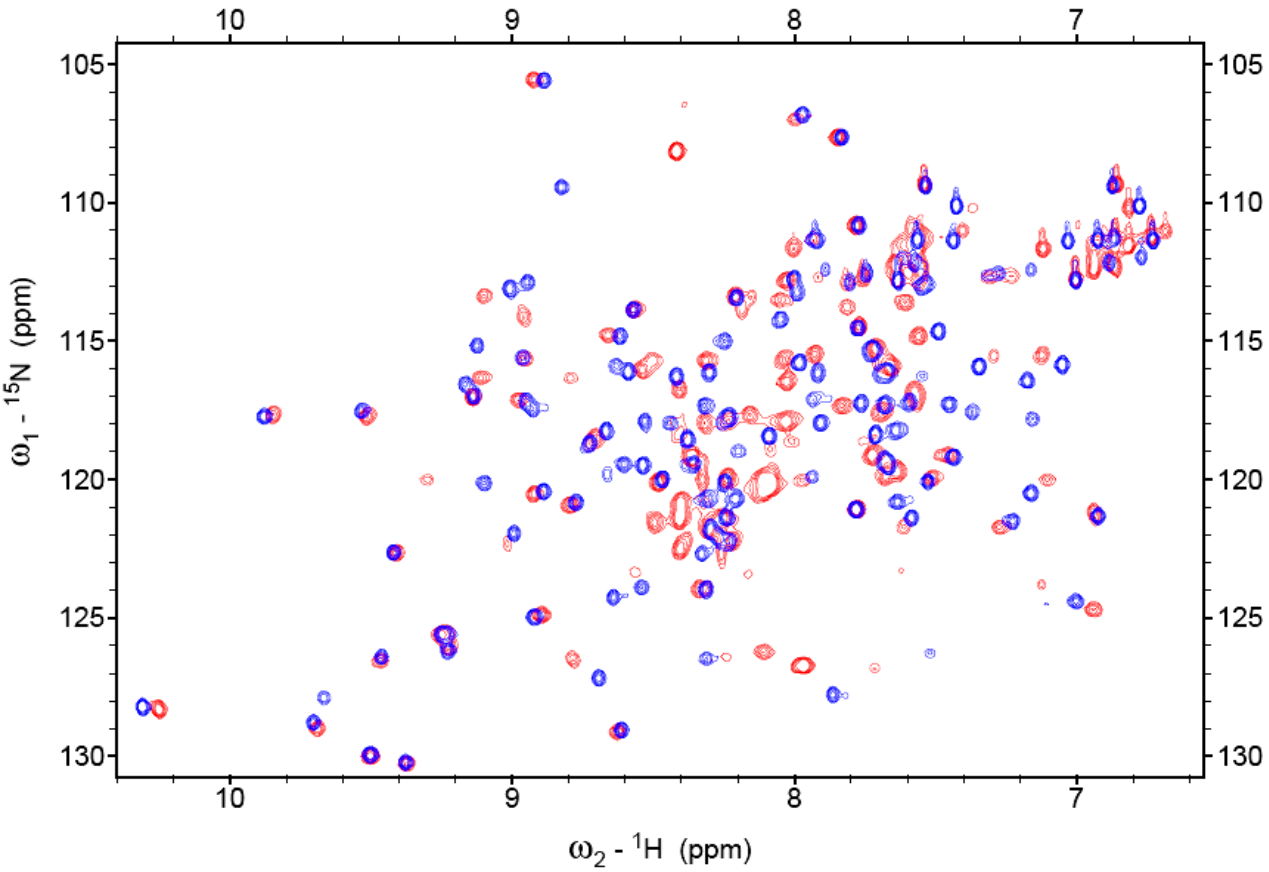

Figure R11. Comparison of the 1H{15N}-heteronuclear single-quantum coherence (HSQC) spectrum of the LD (VAMP7a(1-118)) in blue to that of the LD+SNARE (VAMP7a(1-150)) in red. A number of chemical shifts of the LD vary their resonances in the presence of the SNARE motif, indicating the first direct evidence of a LD-SNARE interaction in VAMP7.

In order to fully interpret this evidence, we performed backbone assignments on the LD and identified each resonance in our LD ^{1}H{^{15}N}-HSQC spectrum. We produced a uniformly ^{15}N, ^{13}C-

labelled LD and performed the following triple resonance experiments: HNCACB, CBCA(CO)NH, C(CO)NH, 3D ^{1}H-^{15}N NOESY-HSQC. Backbone assignment was achieved by connecting sequential C_{α}-C_{β} resonances through the combination of the HNCACB and CBCA(CO)NH (**figure R12**).

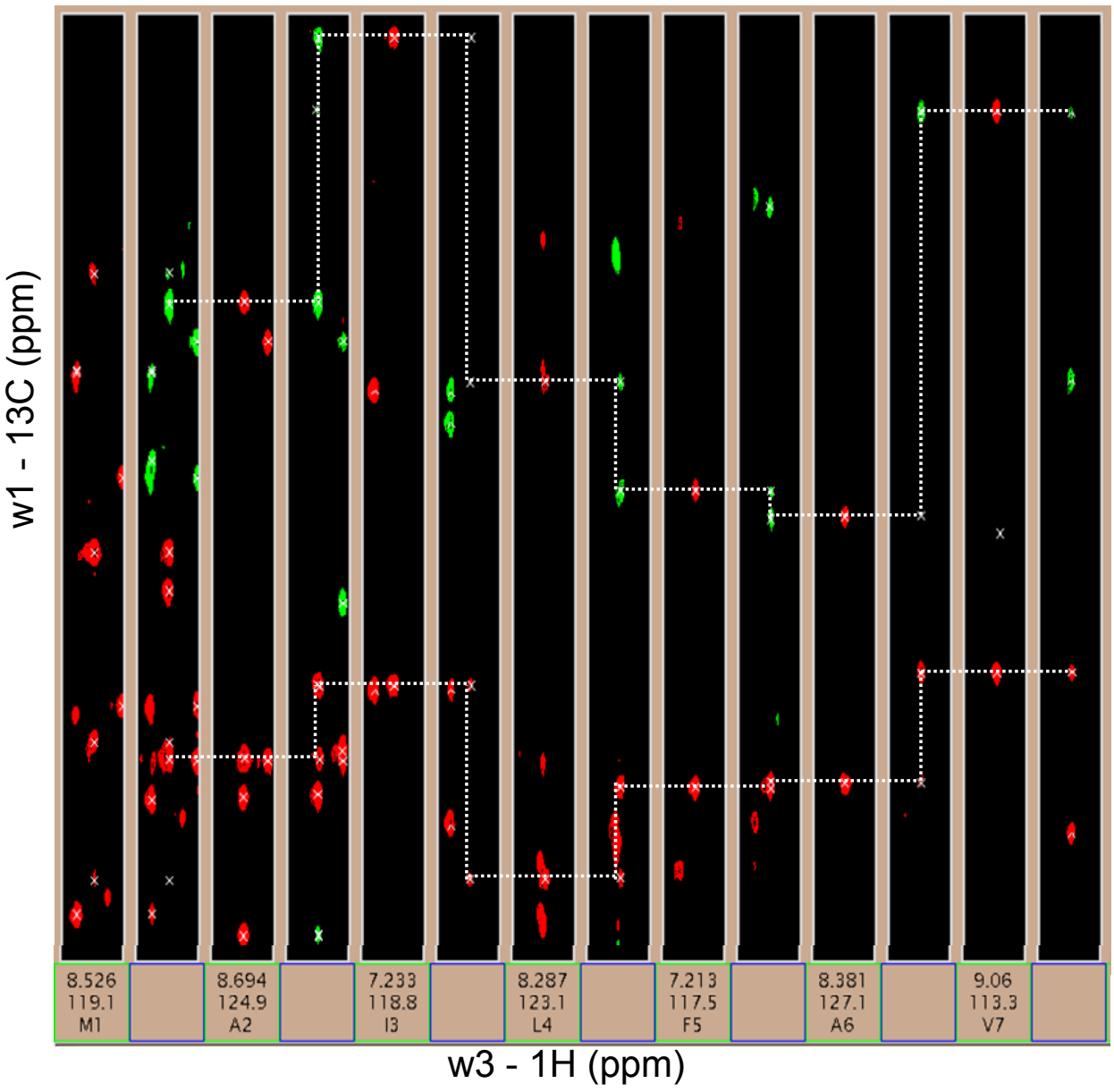

Figure R12: Backbone assignment of VAMP7 LD by connection of sequential Cα-Cβ. (w1-w3) Strips of CBCA(CO)NH and HNCACB spectra are shown for the N-H chemical shifts corresponding to the first 7 N-terminal amino acids of the VAMP7 LD. 14 stripes are arranged in couples that are sequentially aligned from left (first residue, Met 1) to right (last residue, Val 7). Each couple of stripes was taken at the w2 plane corresponding to the ^{15}N chemical shift of the residues indicated below the CBCA(CO)NH stripes in green squares. These latter indeed contain (bottom up): **(i)** amino acid residue in one letter code abbreviation, **(ii)** ^{15}N and **(iii)** ^{1}H chemical shift of the indicated residue. The two segmented, white lines illustrate the connectivities between sequential Cα(lower line)-Cβ(upper line), that yield the assignment of VAMP7a(1-7) fragment.

The analysis of side chain carbon resonances in the C(CO)NH let us resolve ambiguities in C_α-C_β connectivity that were due to peak overlap. ^{1}H-^{15}N NOESY-HSQC was used to review and confirm the assignment by verifying spatial proximity of N-H groups in combination with the 3D structural information already available in the literature [Pryor et al., 2008]. Other than two prolines (prolines do not include amides), only eight residues of the LD could not be assigned in the HSQC spectrum. These residues are distributed in the C-terminus of the molecule, precisely in the α2-α3 loop and in the α3-helix. The absence of strong signals for these residues may be due to conformational exchange in this region, which in a full length native VAMP7 could arise from the C-terminal SNARE motif. We exclude aggregation since the minor dimeric state reported above (see "Biochemical and Biophysical characterization of VAMP7 truncations") showed no major effect on the LD chemical shifts: HSQC spectra acquired at 250 and 100 mM NaCl showed minor, non significant peak shifts (**figure R13**).

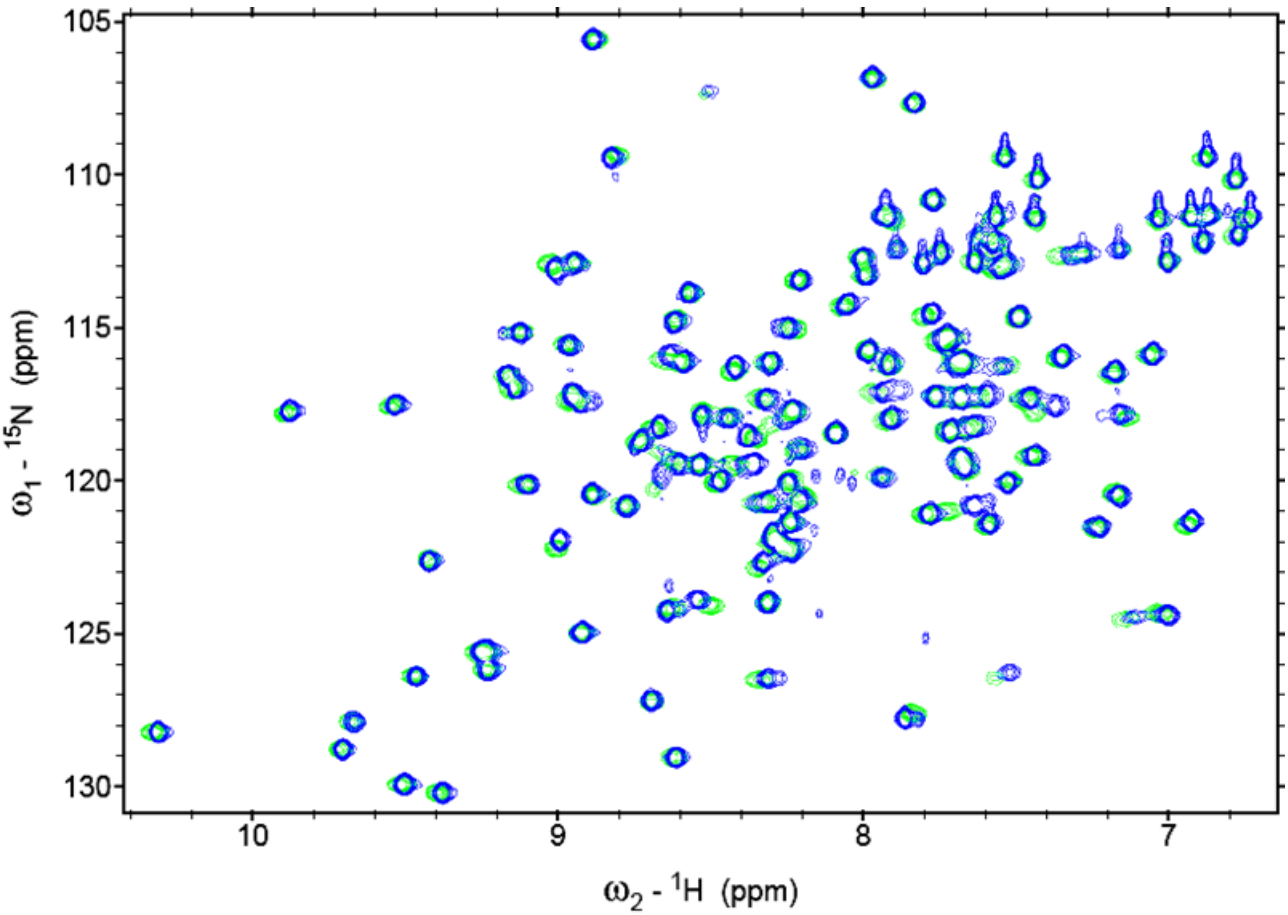

Figure R13. Comparison of the 1H{15N}-heteronuclear single-quantum coherence (HSQC) spectrum of the LD (VAMP7a(1-118)) in 100 mM NaCl (blue) and in 250 mM NaCl (green). The spectra can be considered equivalent as few, minor resonance shifts are observed.

The ability to identify the LD chemical shifts allowed us to analyse the perturbations induced by the interaction with the SNARE motif. For a number of residues localized in the α1-β3 pocket, such as Phe25, Tyr45, His47 and Phe52, large peak shifts or disappearance of peaks (presumably to exchange broadening) were observed. This proved consistent with the previous reports on the LD-SNARE interaction in Ykt6 and Sec22b [Tochio et al., 2001; Mancias and Goldberg 2007] and also with the LD-Hrb interaction shown in VAMP7 [Pryor et al., 2008], and suggested the conservation of this mechanism also for the longin-SNARE domains in VAMP7. However, a large number of LD peak shifts were observed in our spectra, including regions outside the hydrophobic α1-β3 pocket. This evidence likely accounts for all the effects that this interaction has on the LD and not only for those generated on the SNARE-binding site. In other words, the SNARE folding on the LD likely affects not only the chemical environment of those residues of the LD surface that may be directly interacting with the SNARE but also the environment of those facing the SNARE in the wrapping mechanism. In this sense, the X-ray structures of the Sec22b/Sec23-24 complex and the VAMP7-Hrb complex lack this information as they can only monitor the portion of the interaction that is ordered in the crystal.

Due to the number and extent of the peak shifts, and due to peak overcrowding arising from the 32 extra residues of VAMP7a(1-150), the comparison of LD and LD+SNARE HSQC is not completely exhaustive. Peak shifts are not traceable in many cases. This can be addressed by performing backbone assignments on the LD+SNARE VAMP7a(1-150) so that more LD peak shifts can be distinguished and tracked and more information on the LD-SNAMRE interaction can be gained. Approaching the issue from a different angle, we considered whether the LD-SNARE interaction could be reproduced by incubating LD with a synthetic peptide comprising the 9 residues of the putative LD-binding site on the SNARE motif – i.e. VAMP7a(139-150): 139 IMVRNIDLVAQR 150. Such an approach would avoid peak overcrowding by use of non-isotopically labelled peptide (due to the NMR inactivity of the natural abundance ^{14}N nuclei). Other than the practical advantage, it would also tell us whether the LD-SNARE interaction is limited to a *cis* state of the two interacting elements or whether it can exist without the constraint of the native intramolecular LD-SNARE linker. We performed such experiment in a 1:1 and a 1:4 protein:peptide molar ratio but no LD peak shift could be observed. This data suggests the interaction is dependent on the physical restraint comprised by the molecular LD-SNARE linker.

Even if incomplete, the data we showed so far demonstrates the presence of an intramolecular interaction of the SNARE motif onto the LD. This result leaves many new intriguing questions open, since we still lack any dynamic information about this interaction. Is interaction a continuous fluctuation between an “open” and a “closed” conformation of the molecule or is it rather a static

interaction keeping the molecule in a closed, stable state? In other words, are longins distributing between two populations of molecules with either open or closed LD-SNARE conformations, or do they instead group in a single population of closed molecules? More, are these dynamic characteristics homogeneous among the SNARE motif? In order to address these questions we investigated the properties of the LD-SNARE interaction over variation of ionic strength and we analysed the "natural mutation" offered by the VAMP7b splice variant. In particular, we acquired different $^{1}H\{^{15}N\}$-HSQC spectra of VAMP7a(1-150) at different salinity (100, 250, 400, 700, 1000 mM NaCl), as well as VAMP7b(1-150) in 100 mM NaCl. Then, we overlaid these data with the LD chemical shifts – VAMP7a(1-118) – at 100 mM NaCl. Interestingly, the majority of the LD peaks that were perturbed by the SNARE motif at low salt did not revert to the original resonances along with the progressive increase of ionic strength, but rather stayed consistent or even increased their shifts away from the LD resonances (see **figure R14a**). A minority of the LD peaks that were perturbed by the SNARE motif at low salt progressively shifted back to the "SNARE-free" state with increasing buffer salinity (see **figure R14b**). These different behaviours were mapped onto the LD 3D X-ray structure (see **figure R14c**). Surprisingly, the LD peak perturbations that were resistant to high ionic strength were found significantly reduced in recombinant VAMP7b(1-150). In other words, these LD chemical shifts of VAMP7b(1-150) show resonances that are intermediate between the ones of VAMP7a(1-118) and VAMP7a(1-150) (**figure R15a**). VAMP7b(1-150) differs form VAMP7a(1-150) in the last six C-terminal residues (**figure R15b**). These six "natural mutations" likely destabilize the SNARE C-terminus (see "Biochemical and Biophysical characterization of VAMP7 truncations") and affect its ability to coordinate the LD. This data collectively results into some important conclusions. **(i)** VAMP7a LD-SNARE interaction conserves the hydrophobic nature already shown in Ykt6 and Sec22b. In fact, the increase of ionic strength does not disrupt but rather favours the interaction. **(ii)** This interaction is sampled in a fast exchange regime, as demonstrated by the gradual shifting of peak resonances with respect to salt concentration. The latter likely representing a population average of different states that exchange faster than our ability to detect them on the NMR time-scale. **(iii)** VAMP7 molecules are in a dominant closed conformation, as shown by the inability to affect the perturbations of any chemical shifts even at extremely high salinity. These chemical shifts mostly correspond to residues that localize in the LD α1-β3 region. A transition to an "open LD-SNARE state" seems rare for them. **(iv)** Different degrees of flexibility are shown by different portions of the SNARE motif involved in the interaction. In contrast to the fragment that opposes the LD α1-β3 surface, other SNARE motif regions experience a more dynamic interaction, as shown by the possibility to increase their shift perturbations. **(v)** Irrespective of the biological significance of VAMP7b *in vivo*, *in vitro* this protein

represents a variant of VAMP7a with a less stable closed conformation that likely fluctuates between an open and closed state without a strong preference for any of the two.

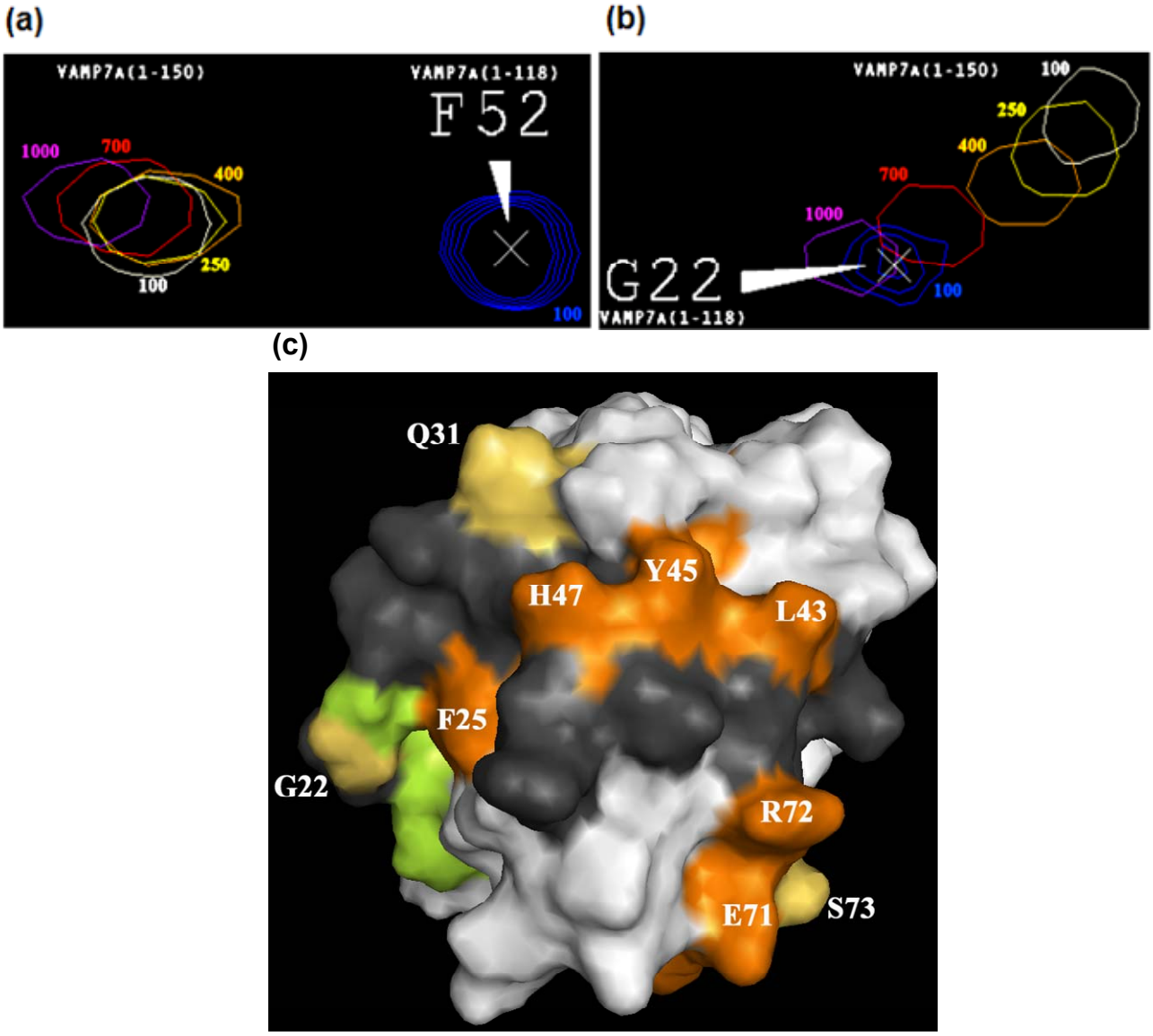

Figure R14. Effect of ionic strength on VAMP7 LD-SNARE interaction. **(a)** Phe 52 is one of those LD residues whose ^{15}N-H chemical shift is perturbed by the presence of the SNARE motif irrespective of different ionic strength in a range from 100 to 1000 mM NaCl. ^{15}N-H Chemical shift of Phe 52 in isolated LD (VAMP7a(1-118)) is shown in blue contour levels; white, yellow, orange, red and violet contour levels illustrate chemical shift of Phe 52 LD+SNARE (VAMP7a(1-150)) in 100, 250, 400, 700, 1000 mM respectively. **(b)** Gly 22 represent an example of the opposite case seen for Phe 52: the resonance perturbation due to the SNARE motif can be progressively reduced by increasing ionic strength – The same color convention apply as in (a). **(c)** The different behaviors seen in (a) (b) are summarized on the LD 3D structure [Pryor et al., 2008], with the orange colored residues being consistent with (a) and the yellow colored ones with (b). Grey residues correspond to those chemical shift that could not be assigned either to (a) or (b) due to signal overcrowding in the spectra. Green colored residues show a similar behavior to (a) that however could be not SNARE dependent. Their resonances in fact show a similar, although weaker, salt-dependency in an isolated LD (see figure R13). Finally, white residues don't show any chemical shift perturbation at all and are likely not interacting with the SNARE motif.

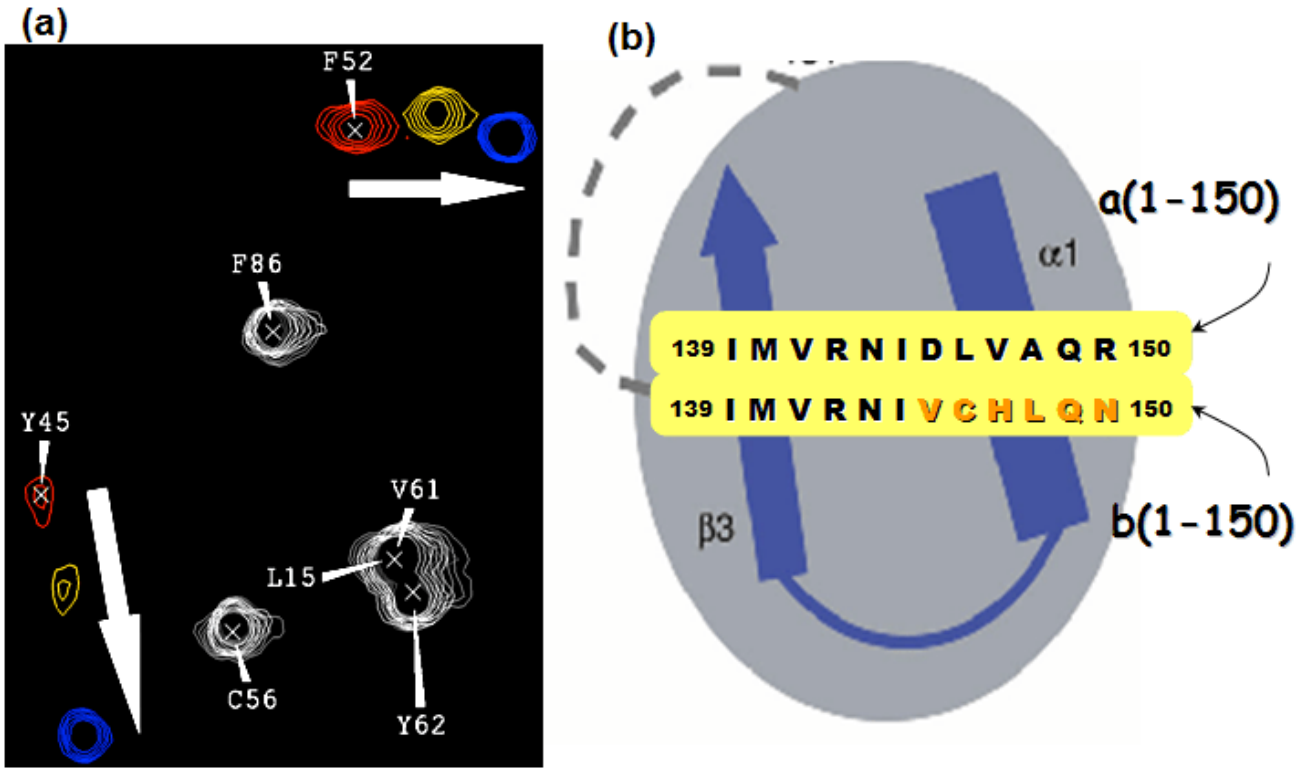

Figure R15. VAMP7b shows a less stable LD-SNARE interaction. **(a)** The same region of three different 1H{15N}-HSQC spectra (all acquired in 100 mM NaCl) is overlaid: VAMP7a(1-118) in blue, VAMP7a(1-150) in red and VAMP7b(1-150) in yellow. Tyr 45 and Phe 52 sense a significantly different chemical environment in the presence of the VAMP7a SNARE motif (wide shift from blue to red peaks). This effect is drammatically reduced (yellow peaks) with the VAMP7b SNARE motif. **(b)** The variantion of amino acid sequence comprised in VAMP7b(1-150) recombinant protein is shown with respect to VAMP7a(1-150). The illustration is analogous to figure R3a.

References

Advani RJ, Yang B, Prekeris R, Lee KC, Klumperman J, Scheller RH.
VAMP-7 mediates vesicular transport from endosomes to lysosomes.
J Cell Biol. 1999 Aug 23;146(4):765-76.

Alberts P, Galli T.
The cell outgrowth secretory endosome (COSE): a specialized compartment involved in neuronal morphogenesis.
Biol Cell. 2003 Oct;95(7):419-24. Review.

Bonifacino JS, Glick BS.
The mechanisms of vesicle budding and fusion.
Cell. 2004 Jan 23;116(2):153-66. Review.

Brunger AT.
Structure and function of SNARE and SNARE-interacting proteins.
Q Rev Biophys. 2005 Feb;38(1):1-47. Epub 2005 Dec 9. Review.

Chen L, Wu H, Sun X, Zhang M, Banfield DK.
Identification of the yeast R-SNARE Nyv1p as a novel longin domain-containing protein.Wen W,
Mol Biol Cell. 2006 Oct;17(10):4282-99. Epub 2006 Jul 19.

Chen X, Lu J, Dulubova I, Rizo J.
NMR analysis of the closed conformation of syntaxin-1.
J Biomol NMR. 2008 May;41(1):43-54. Epub 2008 May 6.

Collins BM, McCoy AJ, Kent HM, Evans PR, Owen DJ.
Molecular architecture and functional model of the endocytic AP2 complex.
Cell. 2002 May 17;109(4):523-35.

Dietrich LE, Boeddinghaus C, LaGrassa TJ, Ungermann C.
Control of eukaryotic membrane fusion by N-terminal domains of SNARE proteins.
Biochim Biophys Acta. 2003 Aug 18;1641(2-3):111-9. Review.

Dietrich LE, Gurezka R, Veit M, Ungermann C.

The SNARE Ykt6 mediates protein palmitoylation during an early stage of homotypic vacuole fusion.
EMBO J. 2004 Jan 14;23(1):45-53. Epub 2003 Dec 11.

D'Esposito M, Ciccodicola A, Gianfrancesco F, Esposito T, Flagiello L, Mazzarella R, Schlessinger D, D'Urso M.
A synaptobrevin-like gene in the Xq28 pseudoautosomal region undergoes X inactivation.
Nat Genet. 1996 Jun;13(2):227-9.

Edeling MA, Smith C, Owen D.
Life of a clathrin coat: insights from clathrin and AP structures.
Nat Rev Mol Cell Biol. 2006 Jan;7(1):32-44. Review.

Fasshauer D, Sutton RB, Brunger AT, Jahn R.
Conserved structural features of the synaptic fusion complex: SNARE proteins reclassified as Q- and R-SNAREs.
Proc Natl Acad Sci U S A. 1998 Dec 22;95(26):15781-6.

Filippini F, Rossi V, Galli T, Budillon A, D'Urso M, D'Esposito M.
Longins: a new evolutionary conserved VAMP family sharing a novel SNARE domain.
Trends Biochem Sci. 2001 Jul;26(7):407-9.

Galli T, Zahraoui A, Vaidyanathan VV, Raposo G, Tian JM, Karin M, Niemann H, Louvard D.
A novel tetanus neurotoxin-insensitive vesicle-associated membrane protein in SNARE complexes of the apical plasma membrane of epithelial cells.
Mol Biol Cell. 1998 Jun;9(6):1437-48.

Gerber SH, Rah JC, Min SW, Liu X, de Wit H, Dulubova I, Meyer AC, Rizo J, Arancillo M, Hammer RE, Verhage M, Rosenmund C, Südhof TC.
Conformational switch of syntaxin-1 controls synaptic vesicle fusion.
Science. 2008 Sep 12;321(5895):1507-10. Epub 2008 Aug 14.

Gonzalez LC Jr, Weis WI, Scheller RH.
A novel snare N-terminal domain revealed by the crystal structure of Sec22b.

J Biol Chem. 2001 Jun 29;276(26):24203-11. Epub 2001 Apr 17.

Hasegawa H, Zinsser S, Rhee Y, Vik-Mo EO, Davanger S, Hay JC.
Mammalian ykt6 is a neuronal SNARE targeted to a specialized compartment by its profilin-like amino terminal domain.
Mol Biol Cell. 2003 Feb;14(2):698-720.

Hasegawa H, Yang Z, Oltedal L, Davanger S, Hay JC.
Intramolecular protein-protein and protein-lipid interactions control the conformation and subcellular targeting of neuronal Ykt6.
J Cell Sci. 2004 Sep 1;117(Pt 19):4495-508.

Jahn R, Scheller RH.
SNAREs--engines for membrane fusion.
Nat Rev Mol Cell Biol. 2006 Sep;7(9):631-43. Epub 2006 Aug 16. Review

Kim YG, Raunser S, Munger C, Wagner J, Song YL, Cygler M, Walz T, Oh BH, Sacher M.
The architecture of the multisubunit TRAPP I complex suggests a model for vesicle tethering.
Cell. 2006 Nov 17;127(4):817-30.

Luzio JP, Pryor PR, Bright NA.
Lysosomes: fusion and function.
Nat Rev Mol Cell Biol. 2007 Aug;8(8):622-32. Review.

Mancias JD, Goldberg J.
The transport signal on Sec22 for packaging into COPII-coated vesicles is a conformational epitope.
Mol Cell. 2007 May 11;26(3):403-14.

Martinez-Arca S, Alberts P, Galli T.
Clostridial neurotoxin-insensitive vesicular SNAREs in exocytosis and endocytosis.
Biol Cell. 2000 Sep;92(6):449-53. Review.

Martinez-Arca S, Coco S, Mainguy G, Schenk U, Alberts P, Bouillé P, Mezzina M, Prochiantz A, Matteoli M, Louvard D, Galli T.

A common exocytotic mechanism mediates axonal and dendritic outgrowth.
J Neurosci. 2001 Jun 1;21(11):3830-8.

Martinez-Arca S, Rudge R, Vacca M, Raposo G, Camonis J, Proux-Gillardeaux V, Daviet L, Formstecher E, Hamburger A, Filippini F, D'Esposito M, Galli T.
A dual mechanism controlling the localization and function of exocytic v-SNAREs.
Proc Natl Acad Sci U S A. 2003 Jul 22;100(15):9011-6. Epub 2003 Jul 9.

Martinez-Arca S, Proux-Gillardeaux V, Alberts P, Louvard D, Galli T.
Ectopic expression of syntaxin 1 in the ER redirects TI-VAMP- and cellubrevin-containing vesicles.
J Cell Sci. 2003 Jul 1;116(Pt 13):2805-16. Epub 2003 May 20.

Matarazzo MR, Cuccurese M, Strazzullo M, Vacca M, Curci A, Miano MG, Cocchia M, Mercadante G, Torino A, D'Urso M, Ciccodicola A, D'Esposito M.
Human and mouse SYBL1 gene structure and expression.
Gene. 1999 Nov 15;240(1):233-8.

Müller DJ, Schulze TG, Jahnes E, Cichon S, Krauss H, Kesper K, Held T, Maier W, Propping P, Nöthen MM, Rietschel M.
Association between a polymorphism in the pseudoautosomal X-linked gene SYBL1 and bipolar affective disorder.
Am J Med Genet. 2002 Jan 8;114(1):74-8.

Pryor PR, Jackson L, Gray SR, Edeling MA, Thompson A, Sanderson CM, Evans PR, Owen DJ, Luzio JP.
Molecular basis for the sorting of the SNARE VAMP7 into endocytic clathrin-coated vesicles by the ArfGAP Hrb.
Cell. 2008 Sep 5;134(5):817-27.

Rossi V, Banfield DK, Vacca M, Dietrich LE, Ungermann C, D'Esposito M, Galli T, Filippini F.
Longins and their longin domains: regulated SNAREs and multifunctional SNARE regulators.
Trends Biochem Sci. 2004 Dec;29(12):682-8. Review.

Rossi V, Picco R, Vacca M, D'Esposito M, D'Urso M, Galli T, Filippini F.
VAMP subfamilies identified by specific R-SNARE motifs.
Biol Cell. 2004 May;96(4):251-6. Review.

Saito T, Parsia S, Papolos DF, Lachman HM.
Analysis of the pseudoautosomal X-linked gene SYBL1in bipolar affective disorder: description of a new candidate allele for psychiatric disorders.
Am J Med Genet. 2000 Jun 12;96(3):317-23.

Schiavo G, Benfenati F, Poulain B, Rossetto O, Polverino de Laureto P, DasGupta BR, Montecucco C.
Tetanus and botulinum-B neurotoxins block neurotransmitter release by proteolytic cleavage of synaptobrevin.
Nature. 1992 Oct 29;359(6398):832-5.

Schlenker O, Hendricks A, Sinning I, Wild K.
The structure of the mammalian signal recognition particle (SRP) receptor as prototype for the interaction of small GTPases with Longin domains.
J Biol Chem. 2006 Mar 31;281(13):8898-906. Epub 2006 Jan 26.

Sutton RB, Fasshauer D, Jahn R, Brunger AT.
Crystal structure of a SNARE complex involved in synaptic exocytosis at 2.4 A resolution.
Nature. 1998 Sep 24;395(6700):347-53.

Takamori S, Holt M, Stenius K, Lemke EA, Grønborg M, Riedel D, Urlaub H, Schenck S, Brügger B, Ringler P, Müller SA, Rammner B, Gräter F, Hub JS, De Groot BL, Mieskes G, Moriyama Y, Klingauf J, Grubmüller H, Heuser J, Wieland F, Jahn R.
Molecular anatomy of a trafficking organelle.
Cell. 2006 Nov 17;127(4):831-46.

Tochio H, Tsui MM, Banfield DK, Zhang M.
An autoinhibitory mechanism for nonsyntaxin SNARE proteins revealed by the structure of Ykt6p.
Science. 2001 Jul 27;293(5530):698-702.

Uemura T, Sato MH, Takeyasu K.
The longin domain regulates subcellular targeting of VAMP7 in Arabidopsis thaliana.
FEBS Lett. 2005 May 23;579(13):2842-6. Epub 2005 Apr 26.

Wen W, Chen L, Wu H, Sun X, Zhang M, Banfield DK.
Identification of the yeast R-SNARE Nyv1p as a novel longin domain-containing protein.
Mol Biol Cell. 2006 Oct;17(10):4282-99. Epub 2006 Jul 19.

Wickner W, Schekman R.
Membrane fusion.
Nat Struct Mol Biol. 2008 Jul;15(7):658-64. Review.

Zhang O, Kay LE, Olivier JP, Forman-Kay JD.
Backbone 1H and 15N resonance assignments of the N-terminal SH3 domain of drk in folded and unfolded states using enhanced-sensitivity pulsed field gradient NMR techniques.
J Biomol NMR. 1994 Nov;4(6):845-58.